Journal of
Synchrotron Radiation

ISSN 0909-0495

Received 8 June 2004
Accepted 29 December 2004

Synchrotron radiation and high pressure: new light on materials under extreme conditions

Russell J. Hemley,* Ho-kwang Mao and Viktor V. Struzhkin

Geophysical Laboratory, Carnegie Institution of Washington, 5251 Broad Branch Road, NW, Washington DC 20015, USA. E-mail: hemley@gl.ciw.edu

With the steady development of static high-pressure techniques in recent years, it is now possible to probe in increasing detail the novel behavior of materials subjected to extreme conditions of multimegabar pressures (>300 GPa) and temperatures from cryogenic states to thousands of degrees. By and large, the growth in this area has been made possible by accelerating developments in diamond-anvil cell methods coupled with new synchrotron radiation techniques. Significant advances have occurred in high-pressure powder and single-crystal diffraction, spectroscopy, inelastic scattering, radiography, and infrared spectroscopy. A brief overview of selected highlights in each of these classes of experiments is presented that illustrate both the state-of-the-art as well as current technical and scientific challenges. The experiments have been made possible by the development of a spectrum of new techniques at both third- and second-generation high-energy sources together with key advances in high-pressure technology. The results have implications for a variety of problems in physics, chemistry, materials science, geoscience, planetary science, and biology.

Keywords: diamond-anvil cells; diffraction; inelastic scattering; radiography; infrared spectroscopy.

1. Introduction

Current technological advances now make it possible to perform experiments on materials subjected to an unprecedented range of pressures, including conditions in excess of those found at the center of our planet (363 GPa, or 3.63 Mbar). With these techniques, condensed phase densities of some materials can be increased over an order of magnitude, causing numerous transformations and new physical and chemical phenomena to occur (Hemley *et al.*, 2002; McMillan, 2002). The growth in this field has been made possible by accelerating developments in both pressure-generating techniques as well as analytical methods with diamond-anvil cells. Arguably, the most significant analytical methods are those based on synchrotron radiation, which has proven to be a uniquely powerful source for diffraction, scattering, and spectroscopy measurements, providing a unique window on materials under extreme conditions. Examples of studies carried out at a variety of synchrotron sources include investigations of dense, solid hydrogen; transformations in molecular materials; novel ceramics; Earth and planetary materials; new types of superconductors, electronic, and magnetic materials; soft matter, liquids and amorphous materials; and biological systems.

Evolving techniques include X-ray diffraction, spectroscopy, inelastic scattering, and radiography (all mainly above 5 keV), as well as infrared spectroscopy. Polycrystalline X-ray diffraction has been the primary technique for high-pressure studies. This includes simultaneous high-P–T diffraction using double-sided laser-heating methods. With newly designed cells that allow variable diffraction geometries, we have been able to collect three-dimensional data to determine stress–strain conditions and the measurement of second-order elastic tensors at ultrahigh pressure–temperature conditions. Single-crystal methods have been extended to above 100 GPa, with the prospect of full crystallographic refinements. Moreover, studies carried out during the past three years provide numerous breakthroughs in high-pressure X-ray spectroscopy. High-pressure X-ray spectroscopy and inelastic scattering have been hindered in the past by insufficient synchrotron radiation intensity and by the opaqueness of high-pressure vessels at crucial X-ray energies. With improvement in X-ray brilliance and the development of X-ray-transparent ultra-high-pressure cell components, a window has been opened for studying local chemical environments, including atomic coordination, structures, and bonding character with a diversity of X-ray spectroscopies and scattering techniques. Other experiments involve the use of X-ray radiography over a range of pressures. Finally, the enormous flux advantage of infrared synchrotron radiation relative to conventional thermal sources provides a significant improvement in spectroscopic studies of microscopic samples at very high pressures. This technique has been crucial for uncovering new phenomena at very high pressures, particularly for molecular systems.

This paper provides an overview of selected developments and current challenges in the study of materials at very high pressures using synchrotron radiation techniques. Although advances made possible by high-energy third-generation sources are particularly notable, new beamline techniques allow experiments at second-generation sources to be competitive and continue to produce significant new results. A growing world-wide community is involved in synchrotron-based high-pressure studies of materials (*e.g.* Katrusiak & McMillan, 2004). An exhaustive review of this expanding field is thus beyond the scope of this paper. Instead, here we examine representative studies in several key areas, focusing on selected recent results from our group that show the interrelationships among the techniques, including complementary information provided by non-synchrotron methods as well as the diversity of scientific problems that can be addressed.

2. Developments in powder diffraction

Polycrystalline diffraction has been the most common technique for high-pressure investigations involving synchrotron radiation and has been used for studies of a broad range of materials. Energy-dispersive diffraction is a low-resolution method, but it has been particularly useful for ultrahigh-pressure investigations as well as studies of low-Z materials because of the ability to spatially filter both the incident collimated or micro-focused X-ray beams as well as the diffracted beams, thereby eliminating or at least greatly suppressing background signal from the surrounding apparatus (*e.g.* anvil and gasket). In contrast, higher-resolution monochromatic angle-dispersive methods employing CCD and image-plate detectors allow high-resolution measurements that make possible powder refinement techniques up to the megabar pressure range. Both methods can be readily combined with variable-temperature studies, including low-temperature cryogenic methods and high-temperature resistive heating techniques (both external and internal) as well as laser-heating methods discussed below. These measurements provide a measure of P–V–T equations of state (EOS), which together with the crystal structure is key to understanding other physical properties of a material. Although EOS determinations by X-ray diffraction have been a major activity in high-pressure research, collection of close-to-hydrostatic data to very high pressures (*e.g.* >50 GPa) is now becoming available (Andrault *et al.*, 1998; Fiquet *et al.*, 1998; Loubeyre *et al.*, 1996). Since above 11 GPa at room temperature all fluids solidify, such experiments require either soft media, such as He, Ne, and H_2, or careful sample annealing (*e.g.* with laser heating). The accuracy of such data is vital for constraining other properties, such as deviatoric strain and high-pressure thermal expansivity, and for identifying structures of novel materials such as the growing number of new superconductors being uncovered on compression of elemental systems.

A major challenge for high-pressure powder diffraction is the measurement of high-quality diffraction data on low-Z systems at megabar pressures, particularly for those systems crystallizing in relatively complex structures. Nitrogen to 100 GPa and variable temperature is an excellent example. Spectroscopic studies, including synchrotron infrared experiments discussed below, have demonstrated that N_2 breaks down to a non-molecular form at 150 GPa (depending on temperature), and persists as a non-molecular narrow-gap semiconductor to at least 240 GPa (Eremets *et al.*, 2001; Goncharov *et al.*, 2000). X-ray diffraction studies, together with Raman measurements, of the phase diagram to 900 K and 100 GPa were carried out using resistively heated diamond cells. These experiments revealed new classes of structures and demonstrated that the phase diagram may be far different than previously thought (Gregoryanz *et al.*, 2002; Lorenzana *et al.*, 2002). Powder diffraction measurements indicate that the new phases are distinct from those of the known γ- and ε-phases of N_2. Additional work is needed to examine whether the structure of θ-nitrogen is polyatomic (Gregoryanz *et al.*, 2002). This is of particular interest in view of the wealth of theoretical predictions of stability of polynitrogen molecules, including the recent theoretical predictions of the stability of polyatomic phases (*e.g.* N_6) in this pressure range (Mattson *et al.*, 2004).

The recent progress on X-ray diffraction is exemplified by the identification of the structure of polymeric nitrogen. Measurements between 70 and 130 GPa indicate that the phase crystallizes in the cubic gauche structure (Eremets, Gavriliuk, Serebryanaya *et al.*, 2004; Eremets, Gavriliuk, Trojan *et al.*, 2004) predicted theoretically (Mailhiot *et al.*, 1992; Martin & Needs, 1986; McMahan & LeSar, 1985). Critical to this work was the use of high-temperature annealing (Eremets, Gavriliuk, Trojan *et al.*, 2004; Gregoryanz *et al.*, 2005) to reduce structural disorder produced on cold compression (Gregoryanz *et al.*, 2001). Problems that remain are the structure of the semiconducting phase above 130 GPa as well as the metallic phase expected above 270 GPa (Eremets *et al.*, 2001; Goncharov *et al.*, 2000; Gregoryanz *et al.*, 2001) and the new phases observed under intermediate P–T conditions mentioned above.

The application of these diffraction techniques has also resolved long-standing controversies regarding the high-pressure structures and phase diagram of sulfur (Fig. 1) (Young, 1991). The phase-transition sequence, first in its non-metallic phases (Degtyareva, Gregoryanz, Somayazulu, Dera *et al.*, 2005) and then in the high-pressure superconducting state (Degtyareva, Gregoryanz, Somayazulu, Mao & Hemley, 2005), demonstrated that it is very different from that previously reported or assumed. Another high-pressure superconductor is oxygen. The structure of this phase (ζ-O_2) (Desgreniers *et al.*, 1990; Shimizu *et al.*, 1998) has not been unambiguously determined, though it is clearly molecular (Goncharov *et al.*, 2003; Weck *et al.*, 2002), and available diffraction data indicate that the phase suggests it is similar to the δ phase (Akahama *et al.*, 1995). Interestingly, questions also surround the structures of the dense insulating phases at lower pressures, including the question of O_4 complexes (Gorelli *et al.*, 1999), and the structure of a new high P–T diatomic phase (Santoro, Gregoryanz *et al.*, 2004).

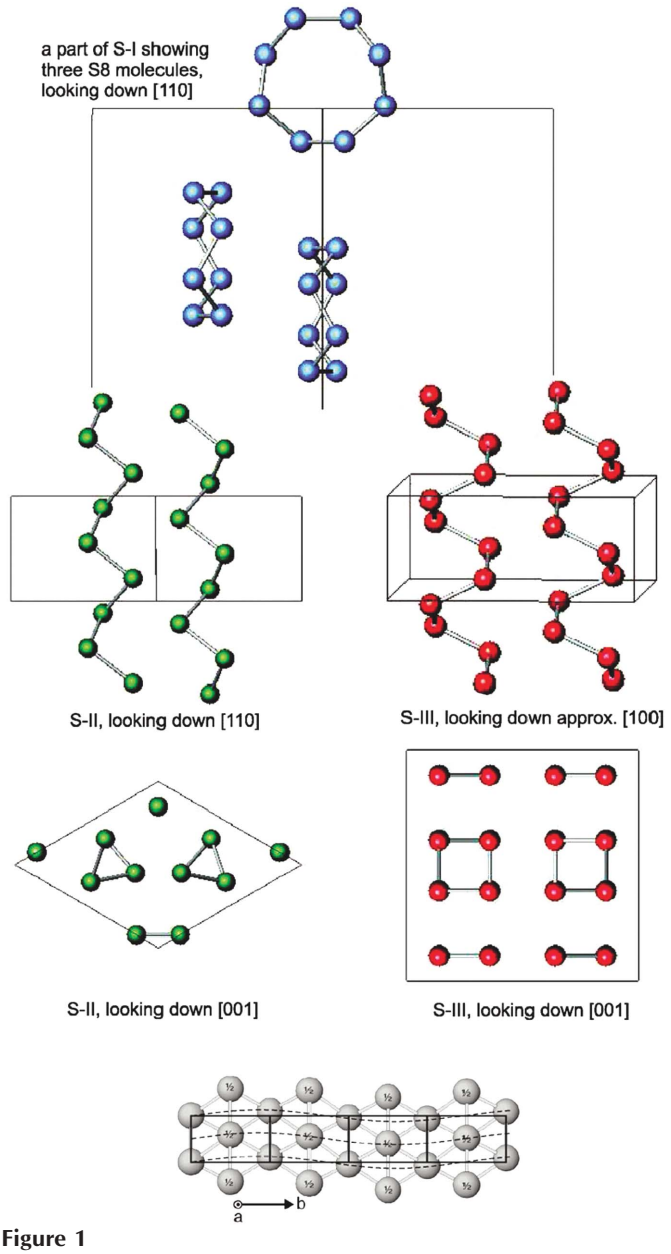

Figure 1
New high-pressure structures of sulfur found by high-pressure powder diffraction. The eight-member rings (S-I, top) break down at 1.5 GPa to form first a triangular chain structure (S-II; left), a novel square chain structure (S-III; right), and then, above 86 GPa, an incommensurate phase (bottom), which is superconducting. A similar sequence is found in Se (Degtyareva, Gregoryanz, Somayazulu, Dera *et al.*, 2005; Degtyareva, Gregoryanz, Somayazulu, Mao & Hemley, 2005).

These results can be compared with systems that are metals under ambient pressure but undergo symmetry-breaking transitions on compression. The Edinburgh group has documented a wealth of findings regarding the formation of complex incommensurate and even self-clathraing behavior in a variety of metals (*e.g.* Degtyareva, McMahon & Nelmes, 2005; McMahon *et al.*, 2000, 2001). Lithium has been predicted to form a paired-atom structure with intriguing similarities to hydrogen (Ashcroft, 2002; Neaton & Ashcroft, 1999, 2001). Symmetry-breaking transformations have indeed been documented by diffraction; the structures differ from those originally predicted theoretically (Hanfland *et al.*, 2000; Takemura *et al.*, 2000), but the pressure range of reported measurements has been limited. Detailed Raman measurements of ^{7}Li and ^{6}Li to 123 GPa at 180 K reveal that new features are consistent with existing structural (Hanfland *et al.*, 2000) and optical changes and interpreted as resulting from a transformation toward a paired state (Goncharov *et al.*, 2005). There is evidence for melting maxima in both Li and Na, with a negative melting line of the latter persisting to above 100 GPa (Gregoryanz *et al.*, 2005).

Powder diffraction measurements have also been instrumental in identifying the new chemical reactions and solid phases formed under pressure. Laser heating of N_2 and Pt at temperatures above 2000 K and pressure above 20 GPa produces PtN (Fig. 2) (Gregoryanz *et al.*, 2004), a novel noble metal nitride crystallizing in the zinc blende structure. This has been identified on the basis of structural refinements on temperature-quenched samples under pressure. Powder diffraction techniques have been essential in identifying novel phenomena in other molecular systems. Densified CO_2 has been the subject of numerous experimental studies (Yoo *et al.*, 1999, 2001, 2002). Laser heating of solid CO_2 followed by X-ray diffraction as well as Raman scattering at 30–80 GPa showed that the compound breaks down to oxygen and diamond, but at pressures higher than 40 GPa the decomposition is preceded by the formation of a new CO_2 phase (Tschauner *et al.*, 2001). Subsequent experiments demonstrate the importance of supplementing the X-ray data with information provided by high-pressure vibrational spectroscopy (Gorelli *et al.*, 2004; Santoro, Lin *et al.*, 2004). N_2O, which is isostructural with CO_2, transforms on laser heating to a novel $NO^+NO_3^-$ structure (Somayazulu *et al.*, 2001). Previously inferred from Raman studies at low pressure, X-ray diffraction following laser heating identified the structure as similar to aragonite ($CaCO_3$), consistent with its proposed ionic nature; a revised interpretation of the structure was made possible by combining energy- and angle-dispersive techniques (*e.g.* Iota *et al.*, 2004; Song *et al.*, 2003). New phases from molecular mixtures have been observed and characterized by X-ray diffraction, including CH_4–H_2O (Chou *et al.*, 2000), Xe–H_2O (Sanloup *et al.*, 2002), and H_2–H_2O clathrates (Mao & Mao, 2004; Mao *et al.*, 2002), and van der Waals compounds (Sihachakr & Loubeyre, 2004).

A different application of the technique has been in the development of a primary pressure calibration scale, which is central to all high-pressure experiments. The commonly used ruby fluorescence pressure scale has high intrinsic precision ($\pm$0.5% in pressure under hydrostatic conditions above 20 GPa) but uncertain accuracy ($\pm$5%) because it is a secondary scale calibrated by less precise ($\pm$5%) primary standards deduced from high-temperature shock-wave data on metals (Mao *et al.*, 1978, 1986). Alternatively, it is possible to develop a primary pressure scale for static compression by combining direct measurements of elasticity and density (*e.g.* Ruoff *et al.*, 1973), but until recently this has been limited to lower pressures. As a simple archetypal oxide and end-member lower mantle mineral, MgO has been the subject of

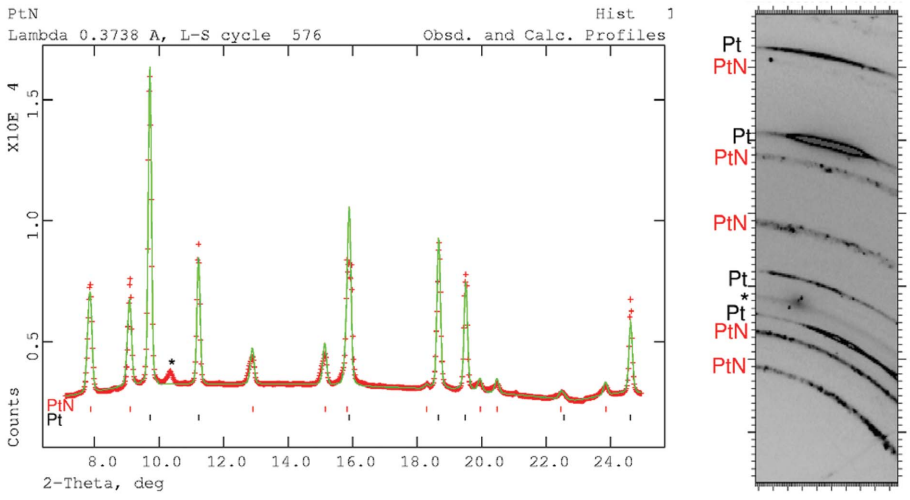

Figure 2
Diffraction pattern of PtN at 20 GPa (300 K) following laser heating. Structure refinement gives the ZnS-type structure. The material can be recovered to ambient conditions (Gregoryanz *et al.*, 2004).

numerous high-pressure studies (*e.g.* Duffy & Ahrens, 1995; Utsumi *et al.*, 1998). Subsequently, the elasticity and 300 K EOS of MgO were studied to 55 GPa by combining synchrotron X-ray diffraction with single-crystal Brillouin scattering in He pressure media (Zha *et al.*, 2000). All second-order elasticity and EOS parameters, including the pressure, were derived without recourse to an independent pressure scale, and the ruby fluorescence was subsequently calibrated using the new MgO primary pressure scale.

The function P (GPa) = $(A/B)[(\lambda/\lambda_0)^B - 1]$ has been used for ruby pressure scales (Mao *et al.*, 1978), with the initial slope fixed at A = 1904 GPa, and B determined by subsequent calibrations. The new results give B = 7.715, which is close to the shock-wave-based calibration for metals in an Ar medium (B = 7.765) (Mao *et al.*, 1986). The ruby fluorescence shift measured against the EOS of W in Ne to 110 GPa by polycrystalline X-ray diffraction (Hemley *et al.*, 1989). It was pointed out that the pressure at 120 GPa based on the EOS of W was systematically higher than that determined from the Ar-based quasihydrostatic ruby scale (*i.e.* 5%). The data fall between the curves with A = 1930, B = 7.765 (Mao *et al.*, 1986) and A = 1918, B = 11.7 estimated the diamond Raman shift extrapolated from below 50 GPa (Aleksandrov *et al.*, 1987). These observations are consistent with recent powder diffraction measurements and theoretical calculations that indicate an underestimation of pressure (Dewaele *et al.*, 2002, 2004; Kunc *et al.*, 2003). In particular, a systematic study of six elements to 150 GPa has been performed by powder (and single-crystal) diffraction (Dewaele *et al.*, 2004). A recent reinvestigation of the MgO pressure scale with higher resolution also shows a higher pressure (Ding, Mao *et al.*, 2005). A systematic study to higher pressure is required to establish a new low-temperature calibration. Extension to combined high-P–T calibration is also of critical importance. In a companion study, an improved P–V–T EOS for MgO was developed (Speziale *et al.*, 2001), and more recently an improved EOS for He was determined, along with the pressure dependence of C_{ij} from Brillouin scattering (Zha *et al.*, 2004). There have also been significant improvements in pressure calibration at simultaneous high pressures and temperatures by resistive-heating/X-ray diffraction of multiple elements (Fei *et al.*, 2004). The extension of self-consistent pressure calibrations to higher pressures and to high-P–T conditions should be carried out with new synchrotron techniques in combination with acoustic velocity methods.

Another challenge is extending microdiffraction to finer and finer spatial resolution. The ability to probe microscopic samples at ultrahigh pressure with high spatial resolution has been extended with the use of X-ray-transparent gaskets that allow a three-dimensional determination of stress and strain under these conditions (Hemley, Mao *et al.*, 1997). The experiment was carried out at an ESRF wiggler with a beam collimated to 5 µm × 5 µm dimensions at the sample, which consisted of Fe and W. With the use of the preformed high-strength gasket, sample pressures in excess of 350 GPa could be reached (*e.g.* determined by the EOS of W), giving a strain anisotropy of order 10% (corresponding to a stress difference of ∼50 GPa) and a surprising enhancement of yield strength of Fe and W. In a second set of experiments, the pressure distribution obtained from diffraction of a Re gasket was mapped out with the same micro-X-ray beam. The pressure distribution initially shows the sharp peaked structure associated with the concentration of pressure at the anvil tip. With increasing load and decreasing bevel angle, the peak broadens as the pressure on the culet edge increases, indicating the gradual loss of the central pressure concentration initially created by the bevel. The pressure distribution determined from gasket diffraction by rastering the sample in two dimensions shows that the pressure falls off rapidly from the central region to the edge of the culet (the rim of the cup) and then decreases smoothly with radial distance from the culet edge. The direct measurement of the macroscopic strain in the diamond tip is discussed in a later section. At the smallest length scales (*e.g.* below 1 µm), samples typically approach the single-crystal domain (see below).

3. *In situ* high-P–T X-ray diffraction with laser heating

An important extension of the above techniques involves the coupling of laser-heating techniques with polycrystalline diffraction for *in situ* measurements under very high P–T conditions. The reliability of such experiments critically depends upon the characteristics of the laser heating (Fiquet *et al.*, 1996; Jeanloz & Kavner, 1996; Manga & Jeanloz, 1997; Mao, Shen, Hemley & Duffy, 1998; Shen *et al.*, 2000). Although the technique has been associated with a number of

controversies, many problems have been solved by the advent of the double-sided ('double hot plate') laser-heating technique (Mao, Shen, Hemley & Duffy, 1998), in which a high-power multimode Nd-YAG or Nd-YLF laser with a flat-top power distribution is directed at the sample from both sides. The method has been improved by combining two YLF lasers in TEM_{00} and (donut) TEM_{01} modes to create a flat temperature distribution to better than 1%. Temperatures on two sides are measured separately with an imaging spectrograph and CCD and equalized by controlling the ratio of beam splitting. Uniform temperatures of 3000 ($\pm$20) K have been achieved in a high-pressure sample of diameter 15 µm and thickness 10 µm. A significantly finer X-ray microprobe beam is used for *in situ* characterization of the sample under these uniform *P–T* conditions. When combined with simultaneous X-ray diffraction, the new laser-heating techniques can be used for *in situ* determination of phase diagrams with increasing accuracy, as well as inelastic scattering (as discussed below). Multilayer sandwich samples, including complex polyphase aggregates, can be laser-heated and X-ray data obtained to deep lower mantle *P–T* conditions; with thick diamond gaskets, core conditions can be also accessed (Zou *et al.*, 2001). Most optically transparent samples (silicates, oxides, and molecular phases) can be heated to the requisite temperatures directly (without the 'hot-plate' coupler) using CO_2 lasers.

Perhaps the most challenging problem in this regard is pushing the *P–T* limits of the technique while at the same time achieving high accuracy in the diffraction measurement. A recent example of the technique is the application to the problem of the stability of (Mg, Fe)O under high *P–T* conditions of the deep lower mantle (Lin, Heinz *et al.*, 2003). These *in situ* studies demonstrated that for realistic geochemical compositions the phase is stable throughout the relevant conditions of the deep lower mantle (Fig. 3). Another example is the continuing study of the phase diagram of iron, which is a necessary starting point for understanding the composition, thermal state, and dynamics of the core. Significant strides in determining the phase diagram of Fe have been made recently using these techniques. *In situ* high-*P–T* synchrotron X-ray diffraction studies to above 160 GPa and 3000 K with double-sided laser-heating techniques demonstrate that the hexagonal-closed-packed phase (ε-Fe) has a wide stability field extending from deep mantle to core conditions (Ma *et al.*, 2004; Shen & Heinz, 1998). This interpretation is consistent with recent shock-wave experiments (Nguyen & Holmes, 2004). However, there are major differences in the temperature dependence of the *c*/*a* ratio between experiment (Ma *et al.*, 2004) and various theoretical calculations (Steinle-Neumann *et al.*, 2001, but also see Gannarelli *et al.*, 2003; Vočadlo *et al.*, 2003); this issue needs to be examined further with higher *P–T* measurements.

Detailed information on crystal structures is an essential starting point for understanding the origin of chemical and physical properties of materials that comprise the Earth's lower mantle. Accurate measurements of multiphase assemblages under high-*P–T* conditions represent another area of future growth. An excellent example, and one critically important for geoscience, is the study of new mineral assemblages that form in laser-heating experiments as well as direct studies of whole rock samples subjected to deep earth conditions. High-*P–T* X-ray diffraction studies to 60 GPa and 2100 K identified the stability fields of the hydrous phase D, phase E, and superhydrous phase B; these phases can serve as reservoirs for water in the mantle but eventually release water by 1200 km in sufficiently cold slabs that may pass into the lower mantle where they break down to form complex assemblages (Shieh, Mao, Hemley & Ming, 2000; Shieh, Mao, Konzett & Hemley, 2000; Shieh *et al.*, 1998; Williams &

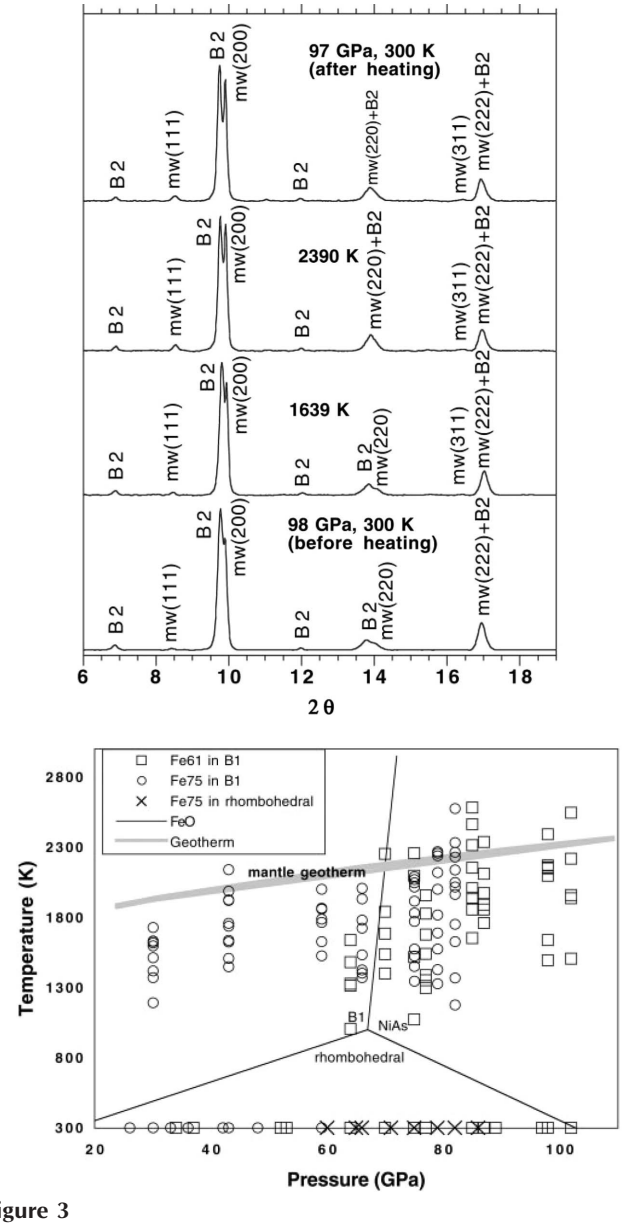

Figure 3
Top: *in situ* X-ray diffraction patterns of $(Mg_{0.39},Fe_{0.61})O$ on laser heating to 2390 K at 98 GPa. A monochromatic beam (wavelength = 0.3311 Å) was used. Bottom: phase diagram for (Mg,Fe)O. Solid lines represent the phase lines for FeO. The grey line shows the approximate mantle geotherm. Open squares and open circles: $(Mg_{0.39},Fe_{0.61})O$ and $(Mg_{0.25},Fe_{0.75})O$ in the B1 structure, respectively; crosses: $(Mg_{0.25},Fe_{0.75})O$ in the rhombohedral structure (Lin, Heinz *et al.*, 2003).

Hemley, 2001). As regards studies of whole rock samples, the phase relations and melting temperatures of natural mid-ocean ridge basalt (MORB) has been studied at mantle pressures up to 64 GPa (Hirose *et al.*, 1999). Perhaps most significant is the extension of these *in situ* high-*P*–*T* diffraction techniques to conditions of the D″ layer and the core–mantle boundary region (*i.e.* 100–135 GPa), where a post-perovskite (ppv) phase of $MgSiO_3$ has been documented (Murakami *et al.*, 2004). It is proposed to have the $CaIrO_3$ (*Cmcm*) structure. The observation has been confirmed by subsequent experimental and theoretical studies (Iitaka *et al.*, 2004; Mao, Shen *et al.*, 2004; Oganov & Ono, 2004; Tsuchiya *et al.*, 2004*a*,*b*). Notably, Fe is found to expand the stability field of the ppv and to lower the transformation pressure (Mao, Shen *et al.*, 2004). *In situ* high-*P*–*T* diffraction studies for the other phases have been carried out [*e.g.* for Al_2O_3 (Lin, Degtyareva *et al.*, 2004)]. There is now a need to examine additional transitions predicted theoretically and the effect of other elements on the stability and structure of ppv (*e.g.* Caracas & Cohen, 2005*a*,*b*) using the high-*P*–*T* techniques now available.

4. Single-crystal X-ray diffraction

Single-crystal X-ray diffraction provides far more complete and accurate information on structure than can polycrystalline diffraction commonly performed at high pressures. In addition, the concentration of diffracted intensity in single-crystal reflections can be crucial for measurements on small amounts of low-*Z* materials at very high pressures (Mao, Hemley *et al.*, 1988; Mao, Jephcoat *et al.*, 1988). The single-crystal EDXD method first used for H_2 to 26.5 GPa (Mao, Jephcoat *et al.*, 1988) was extended to 120 GPa with He separating the sample from the gasket to preserve the integrity of the crystal (Loubeyre *et al.*, 1996). The method has also been used to study H_2O (ice X) embedded in gold to 165 GPa (Loubeyre *et al.*, 1999). As for the powder EDXD method, the polychromatic synchrotron beam allows sufficient spatial filtering of the incident and diffracted beams for measuring minute crystals at ultrahigh pressures above the background from the surrounding apparatus (*e.g.* anvil and gasket). Preliminary low-temperature diffraction was carried out as a part of this study, but only to 100 K and 60 GPa using the cryostat developed for determination of the phase diagram of ^{4}He (Loubeyre *et al.*, 1993). This was subsequently extended to lower temperature; the I–II transition line has been crossed using both single-crystal (Loubeyre, 2003) and powder diffraction (Kawamura *et al.*, 2001), although the limited number of reflections is insufficient to fully constrain the structure; this remains a challenge for future work. A notable result of the X-ray diffraction measurements to 120 GPa was the unexpected high compressibility (Loubeyre *et al.*, 1996). This study used the earlier Ar-based ruby scale, which underestimates pressure. As such, the EOS determined to 26.5 GPa (Hemley *et al.*, 1990) is in better accord with the higher pressures indicated from more recent ruby calibration studies discussed above (see also Hemley & Mao, 2001*b*) The elasticity and EOS of ^{4}He was recently determined using a combination of single-crystal and Brillouin scattering measurements (Zha *et al.*, 2004). As discussed above, single-crystal measurements of the metallic phase of oxygen have been reported (Weck *et al.*, 2002), but the structures have not yet been unambiguously determined.

The technique has also been used to study several minerals to pressures above 30 GPa. The high-*P*–*T* behavior of magnesiowüstite, likely the second most abundant mineral in the Earth's lower mantle, has a direct bearing on the seismological and compositional models of the deep Earth (Lin, Heinz *et al.*, 2003). Studies of phase transitions, including disproportionation and metallization, of magnesiowüstite at high pressures and temperatures are also central to understanding core formation, core–mantle interaction, and inner-core solidification. Magnesiowüstite is arguably the only major component common to both the oxide lower mantle and the metallic core. Under ambient conditions, magnesiowüstite crystallizes in the NaCl (B1) structure. At high pressures, the wüstite end member goes through two phase transitions from B1 through a rhombohedral distortion to the NiAs structure (Mao *et al.*, 1996; Shu *et al.*, 1998) while the MgO end member remains in the B1 structure throughout the *P*–*T* range of the Earth, as discussed above (Duffy & Ahrens, 1995; Duffy *et al.*, 1995). The cubic rhombohedral transition in the iron end member, wüstite at 17 GPa and in magnesiowüstites ($Fe_{0.95}Mg_{0.05}O$ and $Fe_{0.9}Mg_{0.1}O$) near 19 GPa have also been identified. These studies have been extended in a combined high-pressure/variable-temperature X-ray and neutron diffraction study to probe both the crystallographic and magnetic structure across the phase transition (Ding, Xu *et al.*, 2005). Single-crystal studies using the energy-dispersive technique include investigations of the high-pressure behavior of methane hydrates, which provide direct observation of two new phases below 2 GPa (Chou *et al.*, 2000).

Single-crystal measurements provide detailed information on mechanisms of structural transformations. Single-crystal X-ray diffraction of stishovite confirmed (Hemley *et al.*, 2000) the rutile ($P4_2/mnm$) to $CaCl_2$ (*Pnnm*) transition near 50 GPa identified previously by Raman spectroscopy and predicted by first-principles theory (Kingma *et al.*, 1995). Earlier structural studies employed powder X-ray diffraction techniques without a pressure medium (Andrault *et al.*, 1998; Kingma *et al.*, 1996). Single-crystal X-ray diffraction measurements were carried out during compression and decompression to 65 GPa (at room temperature) (Hemley *et al.*, 2000). The spontaneous strains e_1–e_3 for a tetragonal to orthorhombic transition are given by $e_1 = (a - a_0)/a_0$, $e_2 = (b - a_0)/a_0$, and $e_3 = (c - c_0)/c_0$, where a, b and c are lattice parameters of the orthorhombic phase, while a_0 and c_0 are the lattice parameters of the tetragonal phase extrapolated into the stability field of the orthorhombic phase. The order parameter Q scales as $(e_1 - e_2)^2$; as expected it is linear in pressure. All of the spectroscopic, X-ray diffraction, and theoretical results have been combined to develop an order-parameter model for the transition based on Landau theory (Carpenter *et al.*, 2000). The C_{11}–C_{12} instability at the transition gives rise to an anomalous decrease in the shear wave velocity, which provides

a seismic signature that could be diagnostic of free silica in the deep mantle.

Micro X-ray diffraction techniques developed for high-pressure studies have been used to examine a variety of natural samples at ambient pressure. Single-crystal diffraction studies were carried out in coesite inclusions in a suite of diamonds from Venezuela (Sobolev *et al.*, 2000). These revealed confining pressures of 5 GPa that confirmed inferences based on Raman spectroscopy, and provided a new geobarometer for understanding diamond formation. The α-PbO_2 of SiO_2 was identified in the Shergotty meteorite, confirming its high-P–T history and the natural occurrence of this polymorph of silica (Dera *et al.*, 2002). A study of shocked Suizhou meteorite samples led to the discovery of new post-spinel phases of chromite. One appears to be an important marker material in mantle samples (Chen, Shu, Xie & Mao, 2003). In a follow-up study, a second phase was found and complementary high-P–T diamond cell experiments confirmed the P–T range of the transformation and provided information on the shock process of the meteorite (Chen, Shu, Mao *et al.*, 2003). Merrilite was also found to transform to a new high-pressure phase in this meteorite (Xie *et al.*, 2002). A new Fe–Si phase was found in lunar samples (Anand *et al.*, 2004), as discussed below.

Zone-axis diffraction of thin crystals is a powerful technique in transmission electron microscopy, but has seldom been applied with X-rays because it can only be observed with thin crystals using short-wavelength radiation. Unlike normal Bragg diffraction methods, which require rotation of the diamond cell sample, zone-axis diffraction patterns with many reflections that uniquely determine the symmetry of different domains in the sample may be obtained with an appropriately oriented crystal without rotation. The recent observation of zone-axis twinning in $Fe_{1-x}O$ (hereafter called FeO) has confirmed previous interpretations of homoepitaxial relation and mechanism of the phase transition. Moreover, the study reveals that diffuse scattering intensity decreases with pressure and gradually disappears above 17 GPa (Shu *et al.*, 1998), with the formation of coexisting phases of different symmetry at higher pressure. Though related transitions are observed at high temperature (Schweika *et al.*, 1995), this pressure-induced order–disorder transition of defect clusters in FeO at high pressure appears to be unique. The technique has also been applied to (Mg, Fe)O of different compositions to megabar pressures (Jacobsen *et al.*, 2004). Another application of the single-crystal zone-axis diffraction method is for the determination of phonon dispersion. For this method, a beam of monochromatic synchrotron X-rays incident to a thin single crystal creates a rich intensity pattern behind the sample that reflects scattering by thermally populated phonons (Holt *et al.*, 1999). This simple and efficient method is suitable for phonon studies in essentially all materials, and complements the traditional neutron scattering technique. Since the thermal diffuse scattering signal from X-ray transmission scattering is much stronger than the energy loss signal from inelastic scattering methods, it becomes possible to study phonon dispersion in diamond cells using this technique. Preliminary investigations of Si demonstrate the viability of the technique (Ding, Liu *et al.*, 2005). The approach shows great promise to study routinely phonon dispersion at very high pressures, thereby complementing the inelastic scattering methods described below.

There are now efforts underway for a new generation of techniques for structure determination by single-crystal diffraction at megabar pressures (Dera *et al.*, 2004). So far only the peak energy and peak orientation of single-crystal EDXD have been used for determinations of unit-cell parameters; peak intensities needed for complete structure refinements have not been used, in part because of limited access to reciprocal space with 'conventional' megabar pressure cells. Wide-angle diamond cells with beryllium gaskets allow access to the full reciprocal space of the single-crystal sample needed for structure refinements based on single-crystal diffraction in the megabar range (Hemley & Mao, 2002). An alternative approach involves the combination of white-beam (Laue) and monochromatic techniques. Recent integration of the panoramic diamond-anvil cell with synchrotron X-ray micro-diffraction methods (Tamura, Celestre *et al.*, 2002; Tamura, MacDowell *et al.*, 2002) has overcome these limitations (Mao, 2003). The restriction to forward-diffraction geometry ($2\theta < 90^\circ$) severely limits the accuracy. With the 50–5 µm-size X-ray beam typically used to probe samples at 30–200 GPa, the number of crystals covered by the X-ray beam is often too few for good powder diffraction but too numerous for single-crystal diffraction. The new method focuses polychromatic X-radiation to submicrometer size to resolve very small single crystals, and collects Laue spots with an area CCD detector. The panoramic cell allows complete forward, 90°, and back scatterings, while the background signal is minimized by directing the incident X-ray beam through single-crystal diamonds (*i.e.* avoiding the Be seats and gasket). The incident beam can be changed to monochromatic, tuned through the full energy (wavelength) range, and focused to the identical submicrometer spot for d-spacing determination of each Laue spot (Mao, 2003). All polychromatic Laue spots are collected simultaneously from the same X-ray sampled volume, thus reliable for structure determination. The technique has been used at beamline 7.3.3 of ALS to refine and determine the crystal structures of new Fe–Si phases identified in a lunar meteorite (Anand *et al.*, 2004) (Fig. 4). The technique is readily extended to ultrahigh pressure.

5. High-pressure elasticity from radial X-ray diffraction

The above methods have been extended with the introduction of a new class of high-pressure diffraction techniques employing radial diffraction geometry (Singh *et al.*, 1998). In these experiments samples are investigated under a deliberately imposed deviatoric stress field, providing rich information about strength, elasticity and rheology that is unavailable with hydrostatic experiments (Fig. 5). By the use of radial X-ray diffraction (RXD), the d-spacings as a function of the angle (φ) to the diamond-cell axis are obtained from $\varphi = 0^\circ$ to 90°, $d(hkl) = d_P(hkl)[1 + (1–3\cos^2\varphi)\,\vartheta(hkl)]$, where the

intercept $d_P(hkl)$ denotes the d-spacing under hydrostatic stress σ_P, and the slope $\vartheta(hkl)$ is the lattice strain under the uniaxial stress condition. The hydrostatic pressure is related to σ_3, the axial stress, and σ_1, the radial stresses, by $\sigma_P = (\sigma_3 + 2\sigma_1)/3$. The hydrostatic EOS defines the relation between $d_P(hkl)$ and σ_P. These data can be used to determine the deviatoric stress (given as the uniaxial component) $t = \sigma_1 - \sigma_3$, and shear modulus $G = t/(6\vartheta)$.

Recent applications have addressed particularly important problems in geophysics. Seismological observations of inner-core anisotropy and structure present new questions about the dynamics and magnetism of the core. The anisotropy has been interpreted as a manifestation of elasticity, preferred orientation, and texture of ε-Fe. The experiments on Fe up to 300 GPa described above revealed variations in d-spacings at different sample orientations (Hemley, Mao *et al.*, 1997), indicating non-hydrostatic stresses in the range of 10%. The subsequent experiments were used to estimate the shear modulus of ε-Fe; the RXD result agrees with ultrasonic measurements in a multi-anvil apparatus at 16.5 GPa (Mao, Shu *et al.*, 1998). The aggregate longitudinal velocity (V_P) and shear velocity (V_S) at high P–T are the primary data obtained from seismic observations. They can be determined experimentally from the bulk modulus and density by hydrostatic EOS studies, and G, the shear modulus, by RXD, from $K/\rho = V_P^2 + (4/3)V_S^2$ and $G/\rho = V_S^2$. Determination of G by RXD requires an intricate sample configuration with a layer of stress standard having the same σ_3 as the sample.

The RXD measurements also provide information on single-crystal elasticity. Care must be exercised to separate the effects of plasticity on the inferred elastic constants (Merkel, Yagi *et al.*, 2004; Weidner *et al.*, 2004). The $\vartheta(hkl)$ of ε-Fe over a wide pressure range shows a strong (hkl) dependence, *i.e.* a strong strain anisotropy. Since strain is a product of elasticity and stress, this reflects the combination of elasticity anisotropy and/or stress anisotropy. The complete elasticity tensors (C_{11}, C_{12}, C_{13}, C_{33}, and C_{44}) and the orientation dependence of velocities (V_P, V_{S1}, and V_{S2}) of high-pressure ε-Fe were calculated from the RXD data at the isotropic stress limit (Mao, Shu *et al.*, 1998). However, the validity of the calculation depends on the isostress assumption. The problem can be resolved by using soft but not entirely hydrostatic pressure media to develop a deviatoric stress significantly below the minimum yield strength of iron, thus avoiding the stress

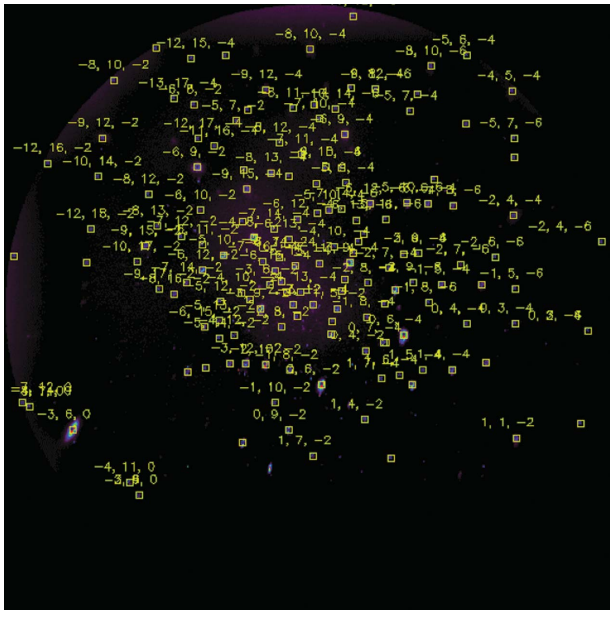

Figure 4
Laue X-ray diffraction pattern of Fe_2Si, a new phase from a lunar meteorite. The pattern is indexed as hexagonal, with $a = 11.6957$ Å and $c = 4.7435$ Å. (From Anand *et al.*, 2004.)

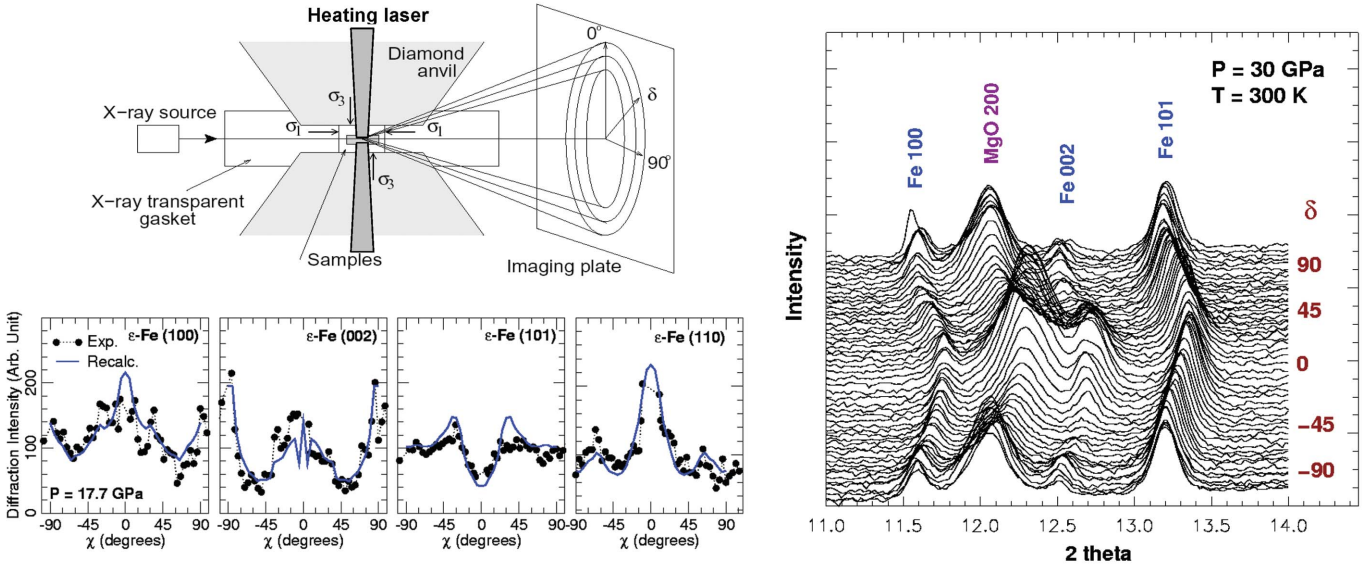

Figure 5
Radial X-ray diffraction in diamond-anvil cells. Top left: schematic of the technique. Bottom left: diffraction patterns showing the texture after the α–ε transition of Fe. Right: diffraction patterns measured for a sample of Fe and MgO (Merkel, Wenk *et al.*, 2004).

anisotropy [(*hkl*) dependence of stress]. The effect of texture on the determination of the single-crystal moduli has been examined and found to be significant for crystal systems more complex than cubic. An inversion method that takes into account texture effects was proposed for ε-Fe (Matthies *et al.*, 2001). Additional constraints have been provided by NRIXS (Struzhkin, Hemley *et al.*, 2004), as discussed below, as well as by Raman spectroscopy (Merkel, Goncharov *et al.*, 2000).

More recent work has involved the use of high-resolution imaging-plate detector and monochromatic X-rays at the ESRF and APS. We studied two main end-member phases of the lower mantle, MgO and $(Mg_{0.9}Fe_{0.1})SiO_3$-perovskite, at ambient T up to 47 GPa and 32 GPa, respectively (Merkel *et al.*, 2002, 2003). We demonstrated that the elastic moduli of MgO obtained with the radial diffraction method are in agreement with the more precise Brillouin spectroscopy studies. The techniques have also been used to study the high-pressure elasticity of metals (Duffy, Shen, Heinz *et al.*, 1999; Duffy, Shen, Shu *et al.*, 1999), oxides (Merkel *et al.*, 2002; Shieh *et al.*, 2002), and other mantle minerals (Kavner, 2003; Kavner & Duffy, 2001).

6. Texture and rheology at very high pressures

Such measurements also reveal rheological information, including deformation mechanisms, preferred orientation, slip systems, plasticity, failure, and shear strength. These measurements have been important for understanding the dynamics and processes associated with texture development in the inner core (Karato *et al.*, 2000). Seismic anisotropy reflects oriented texture in elastically anisotropic minerals. In the aforementioned experiments on Fe to 220 GPa (Mao, Shu, Shen *et al.*, 1998), strong strain anisotropy was observed that corresponded to variations in diffraction intensities and suggest the presence of crystallographic preferred orientation. From the regular changes in intensities as a function of sample orientation, the orientation distribution for ε-Fe was calculated (Wenk *et al.*, 2000). The distribution exhibits a strong concentration of c axes parallel to the axis of the diamond-anvil cell (five to seven multiples of a random distribution). Assuming that this pattern was attained during axial compression, it provides insight into deformation mechanisms at high pressure. Polycrystal plasticity theory predicts c axes parallel to the compression direction as a result of basal slip, if basal slip is either the primary or secondary slip system. These deformation experiments at inner-core pressures provide information about flow processes within the Earth (Poirier & Price, 1999) and are relevant to possible development of anisotropy during outer-core convection.

The uniaxial stress component in the polycrystalline MgO sample is found to increase rapidly to 8.5 ($\pm$1) GPa at a pressure of 10 ($\pm$1) GPa in all experiments (Fig. 5). The uniaxial stress supported by the perovskite aggregate is found to increase continuously with pressure up to 10.9 ($\pm$1.9) GPa at 32 ($\pm$1) GPa. A comparison between the experimental textures and results from polycrystal plasticity suggest that the preferred orientation of MgO is due to deformation by slip in the $\langle 1\bar{1}0\rangle$ slip system under very high confining pressure at room temperature. Under axial compression, a strong cube texture developed in MgO which could be the source of seismic anisotropy. On the other hand, our measurements show no development of significant lattice preferred orientations in the perovskite sample, indicating that deformation by dislocation glide is not the dominant deformation mechanism under these conditions. Assuming that the underlying cause for seismic anisotropy in the deep Earth is elastic anisotropy combined with lattice preferred orientation, our results indicate that silicate perovskite deformed under the conditions of this experiment would not be the source of seismic anisotropy. Subsequent work has examined texture development of more complex polyphase assemblages at high pressure following laser heating (Merkel, Yagi *et al.*, 2004; Pehl *et al.*, 2003).

Both elasticity and rheology is highly temperature and time dependent. Extending the radial X-ray diffraction experiments to high-P–T conditions of the Earth's deep interior with laser heating is an important challenge. Studies of α (b.c.c.) and ε-Fe with angle-dispersive radial X-ray diffraction measurements have been performed to 30 GPa and 1000 K in laser-heated diamond cells (Merkel, Wenk *et al.*, 2004). α-Fe is found to develop preferred orientation compatible with observations under ambient conditions. The preferred orientation of the b.c.c.-phase is inherited by the ε-phase in accordance with the Burgers orientation relationship, consistent with the martensitic nature of the phase transition. A comparison between the observed texture in ε-Fe with results from polycrystal plasticity modeling suggests that the predominant deformation mechanisms are basal slip $\{0001\}\langle\bar{1}2\bar{1}0\rangle$ and prismatic slip $\{10\bar{1}0\}\langle\bar{1}2\bar{1}0\rangle$, presumably associated with minor mechanical twinning. We do not observe evidence of slip on the $\{11\bar{2}1\}\langle 11\bar{2}3\rangle$ system that was proposed based on analogy to Cr–Ni alloys.

7. High-pressure diffraction of amorphous materials

Changes in local structure (radial distribution functions) of amorphous materials at high pressure can be identified by X-ray diffraction for solids (*e.g.* glasses) and liquids (Katayama *et al.*, 2000; Meade *et al.*, 1992; Shen *et al.*, 2003). The spatial resolution provided by EDXD is especially useful for reducing the background signal, which is essential for the accurate measurements of the diffuse amorphous diffraction from small samples of weak scatterers. At very high pressures, the sample thickness is typically only 0.01–0.001 that of the diamond; the background caused by scattering from the diamond anvils may overwhelm the diffraction from the weakly scattering sample. In early applications of this technique, the X-ray structure factor, $S(Q)$, of SiO_2 glass was measured to 42 GPa in the diamond cell (Meade *et al.*, 1992). Large changes in the first sharp diffraction peak of $S(Q)$ with increasing pressure indicate structure transitions in long-range ordering of the glass. Between 8 and 28 GPa the coordination of Si also increases above 4, and approaches 6 at 42 GPa. More recently, the evolution of the structure of GeO_2 was determined with a combination of synchrotron X-ray and neutron

diffraction techniques (Guthrie *et al.*, 2004) together with new large-volume moissanite anvil cell methods (Xu *et al.*, 2004). The X-ray measurements were carried out using high-energy monochromatic methods to obtain data to very high Q and reveal the transition from tetrahedral to octahedral coordination and the extent of intermediate range order in the high-pressure amorphous form (Fig. 6).

An area of particular growth is direct measurements of the effects of pressure (and temperature) on liquid structure. The structure factor of liquid water has been measured to 10 GPa (at variable temperature, and with larger samples) using monochromatic radiation and angle-dispersive methods (Eggert *et al.*, 2002). Recent diffraction studies of molten Fe and Fe alloys to >2300 K have been performed with Paris–Edinburgh cells (Sanloup *et al.*, 2000*a*,*b*). High-P–T X-ray measurements of molten iron reveal structural changes in the liquid up to 5 GPa and 2500 K (Sanloup *et al.*, 2000*a*). These observations may be related to subsequent observations of a viscosity change in the liquid by X-ray radiography under comparable conditions (Terasaki *et al.*, 2002). Recently, the effect of pressure on the structure of the liquid has been examined to above 60 GPa at temperatures above 2000 K using laser-heating diamond cell methods (Shen *et al.*, 2004). Though these data show evidence for continuous structural changes, the reported transformations at lower pressure, as well as those under higher P–T conditions (Alfè *et al.*, 2000; Brazhkin & Lyapin, 2000), need to be examined further; the latter are particularly important for characterizing the state of liquid iron in the outer core. New large-volume diamond-anvil techniques will be crucial for extending these techniques to more complex liquids and to higher P–T conditions.

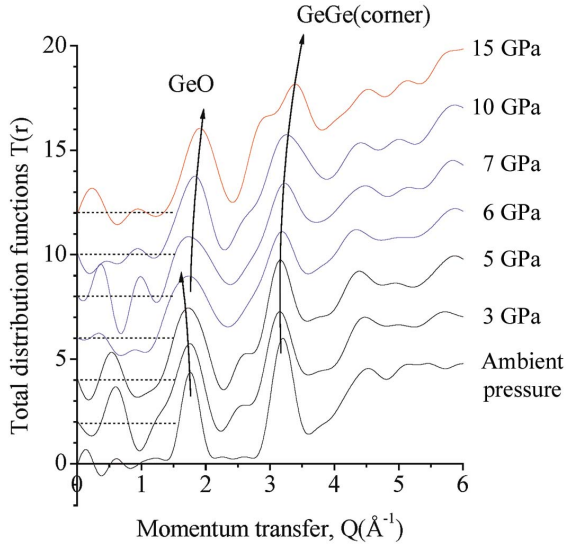

Figure 6
X-ray total radial-distribution functions $T(r)$ up to 15 GPa describe changes in both the local and intermediate-range structure up to ~6 Å. The peak that appears at 3 GPa at around 2.5 Å is identified as a new Ge–O correlation. Above the transition pressure of 6 GPa, the covalent Ge–O peak broadens significantly and is asymmetric at 7 GPa. At 10 GPa, the Ge–O peak again becomes more symmetric, and has shifted to higher r. The local correlations in the glass at 15 GPa closely resemble that of the crystalline rutile structure. Complementary neutron diffraction measurements were carried out in the same material (Guthrie *et al.*, 2004).

8. Radiography at very high pressures

Another technique is transmission radiography, which has been applied for direct measurements of volume in EOS studies, for liquids and amorphous materials most notably in the low-pressure range (<5 GPa) with large-volume cells (Sanloup *et al.*, 2000*b*). Radiography has been used to measure the viscosities. For example, pure liquid Fe at high pressure and temperature has been studied in a large-volume press using the falling/rising sphere technique, allowing for the derivation of sample viscosity through a modified form of Stokes' equation. The effect of pressure on viscosity is fit by the semi-empirical framework for transport coefficients in liquid metals, providing experimental verification of constant viscosity at the pressure-dependent melting temperature of liquid Fe. This falling-sphere approach was used in the viscosity study reported above (Terasaki *et al.*, 2002). Another application of radiography has been for the direct determination of EOS of liquids. Such techniques are being adapted for higher-pressure measurements with diamond cells (Shen *et al.*, 2002), techniques that will benefit significantly by the increase in sample volume made possible with larger anvils discussed below.

X-ray radiography has also been applied to study the macroscopic strain of diamond anvils at ultrahigh pressure, in concert with the ultrahigh-pressure stress–strain measurements described above (Hemley, Mao *et al.*, 1997). In this method, the transmission of a fine X-ray beam perpendicular to the diamond culet is monitored while the culet is scanned across the beam. Because of the great contrast in absorption coefficients of diamond and gasket materials [*e.g.* rhenium (Re) or stainless steel], the transmission intensity profile reflects the thickness of the gasket and the shape of the diamond tips (Fig. 7). Single beveled diamond anvils with small central flats of 10 μm and a rhenium gasket were used. Initially at zero pressure, the combined bevel angle was 17°. The central sample thickness was only 3 μm after gasket indentation, while the edges of the culets of the two diamonds were separated by 45 μm of Re. Because the Re gasket strongly absorbs X-rays, the magnitude of the transmission at a point measured with the 5 μm × 5 μm X-ray beam gives the thickness of the gasket as determined by plastic flow of the metal and the concomitant elastic deformation of the anvil. With increasing load, the 17° combined angle at the anvil tip begins to decrease; that is, the anvil tip begins to flatten. At the highest loads, however, the originally straight slope of the bevel transforms to a cup, with the bevel angle reversed at the edge. Rastering the sample position in two dimensions perpendicular to the X-ray beam provides more detailed information. With the spatial resolution provided by the small X-ray beam, detailed features of the anvil surface, including the 16 facets of the brilliant cut of the diamond, are apparent. The image of the diamond tip shows that a large amount of macroscopic strain can be accommodated by the cupped anvil

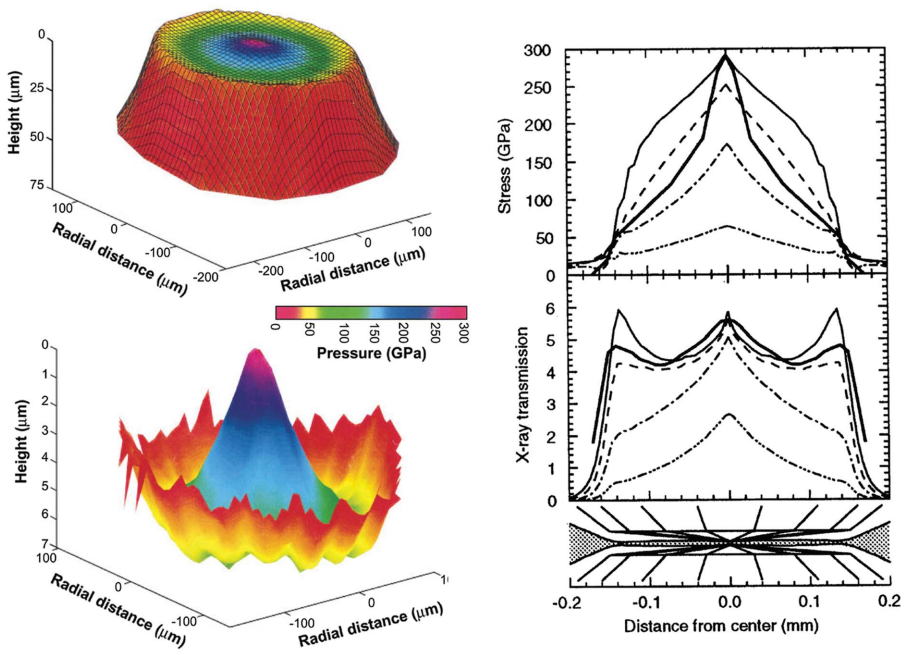

Figure 7
Deformation of diamond anvils at ultrahigh pressure. Left: imaging of stress and deformation from a combined radiography and microdiffraction showing the elastic cupping of a bevelled anvil. The lower image is detail of the tip (Hemley, Mao *et al.*, 1997). Right: two-dimensional view of the deformation and pressure distribution obtained by finite-element modeling of the experimental observations (Merkel *et al.*, 1999).

tip. With the edges of the two anvils approaching, further loading only increases pressure at the edge and causes catastrophic diamond failure. The cupping in the transmission radiograph can thus be used as a signal to stop further loading and save the diamonds. Finite-element modeling calculations of these observations (Merkel *et al.*, 1999; Merkel, Hemley *et al.*, 2000) provide guidance in the development of the next-generation cells, including methods for increasing sample volume, improving device stability, and advancing to still higher pressures.

9. High-pressure X-ray emission spectroscopy

An array of high-pressure X-ray spectroscopic techniques have now come on line to supplement the aforementioned diffraction experiments. Advances in this area have come about as a result of the new generation of high-energy synchrotron sources, high-strength and X-ray transparent (Be and composite Be–B) gaskets, as well as new cell designs. These developments allow spectral measurements under extreme pressures down to 4 keV, which covers the important K edge of transition elements and L edge of rare-earth elements. Among these are methods that extend the range of conventional spectroscopic methods such as optical absorption (*e.g.* crystal-field) spectroscopies (Hemley, Mao & Cohen, 1998). The spin state of iron can be determined by the analysis of the Fe K_β emission line. The emission spectrum of high-spin iron is characterized by a main peak with an energy of 7058 eV, and a satellite peak located at lower energy due to the 3*p*-core/3*d*-hole exchange interaction in the emission final state. In the 2+ oxidation state of iron (d^6 configuration), the low-spin state is characterized by a total magnetic moment equal to zero. This collapse of the 3*d* magnetic moment has a distinct signature, since the exchange interaction (and therefore the lower-energy satellite) vanishes and the resulting spectrum consists of a single narrow line.

The technique was first applied at high pressure to FeS, where the high-spin/low-spin transition was identified at 7 GPa (Rueff *et al.*, 1999), and to FeO, which has been studied to 143 GPa (Badro *et al.*, 1999). X-ray diffraction was combined with the emission measurements to give the structure (which was rhombohedral at the highest pressures). In contrast, Fe_2O_3 undergoes a high- to low-spin transition near 60 GPa (Badro *et al.*, 2002). The emission spectrum in the region of the valence band reveals information on the width of the band. This part of the spectrum provides a direct measure of the symmetry-projected anion *p* bandwidth. The results also show that the symmetry-projected local electronic density of states (DOS) of the valence band does not broaden, consistent with a preserved high-spin state. In order to reconcile these observations with previous Mössbauer data (Pasternak *et al.*, 1997), there must be a maximum T_N above 300 K and 40–60 GPa with re-entrant behavior back to the paramagnetic phase above 80 GPa (Badro *et al.*, 1999). Combined laser-heating/X-ray-diffraction measurements show that the low-spin state can be quenched from high temperature at 150 GPa (Struzhkin, Hemley & Mao, 2004). The electronic (Badro *et al.*, 1999; Pasternak *et al.*, 1999) and crystallographic transitions in Fe_2O_3 appear to be distinct (Badro *et al.*, 2002). High-pressure X-ray diffraction and X-ray emission measurements on Fe_3C were performed (Lin, Struzhkin, Mao *et al.*, 2004). NRIXS measurements on Fe_3S and Fe–Si and Fe–Ni alloys constrained thermodynamic properties and magnetic transitions (Lin, Fei *et al.*, 2004; Lin, Struzhkin *et al.*, 2003).

Most recently, the technique has been applied to more chemically complex deep Earth minerals, (Mg,Fe)O [magnesiowustite (mw)] and $(Mg,Fe,Al)SiO_3$ perovskite. The high-spin/low-spin transitions in (Mg,Fe) solid solutions are expected to have profound implications for compositional layering in the lower mantle because the transition may shift iron-partitioning towards mw, possibly resulting in a more equal distribution of Fe/Mg above the transition, with a more Fe-rich mw (Fe-poor perovskite) below the transition in the lower mantle. The low-spin iron, with an ionic radius reduced by as much as 10–20%, behaves effectively like a new element in geochemical processes. We recently found a correlation

between the high-spin/low-spin transition and density anomalies (changes in equation of state) in mw (Lin, Struzhkin, Jacobsen *et al.*, 2004). An abrupt transition was found in (Mg,Fe)O at 60 GPa (Badro *et al.*, 2003). In contrast, a gradual transition was found beginning around 100 GPa in the silicate perovskite (Badro *et al.*, 2004; Li *et al.*, 2004).

10. Nuclear resonance inelastic and nuclear forward scattering

Traditionally, measurements of phonon density of states (DOS) have been limited to the realm of neutron inelastic scattering, which requires centimeter-size samples currently impossible for ultrahigh-pressure research. The nuclear resonant inelastic X-ray scattering (NRXIS) technique has been developed for the measurement of phonon DOS of samples containing ^{57}Fe (Seto *et al.*, 1995; Sturhahn *et al.*, 1995). The technique is particularly suitable for pure iron in which all phonons naturally result from vibrations of Fe atoms; experiments at ambient pressure demonstrate that the measurement provides an unbiased representation of the true DOS as shown by detailed comparison of neutron scattering and NRIXS for α-Fe. However, high-resolution NRIXS is a low-count-rate experiment even for optimal sample sizes under ambient conditions with a third-generation synchrotron undulator source, which makes ultrahigh-pressure experiments challenging because of their microscopic samples.

The first phonon DOS studies using NRIXS in the megabar range were carried out on Fe up to 153 GPa at 300 K (Mao *et al.*, 2001). The wide-angle diamond cell was used for achieving acceptable counting rates (>0.1 counts s^{-1}) above 100 GPa. The long piston-cylinder configuration is used to assure alignment stability that is critical for reaching ultrahigh pressures. Very wide lateral openings on the cylinder (except three thin 15° webs connecting the cylinder with the end) allow maximum collection of the Fe fluorescence signal around the belt at ±34° from the sample plane perpendicular to the diamond-anvil axis. This belt covers the entire accessible solid angle around the sample as the diamond anvils, which are nearly opaque to the low-energy Fe fluorescence emission, necessarily occupy the remaining two conical solid angles. High-strength Be gaskets were used and provide side windows for the low-energy Fe K_α (6.4 keV) and K_β (7.1 keV) fluorescence. Enriched ^{57}Fe samples of diameter 25 µm are placed at the center of the gasket hole without any additional pressure medium. The high-resolution (2 meV) monochromator scans the range of ±100 meV at steps of 0.4 meV in reference to the 14.4125 keV nuclear resonance absorption of ^{57}Fe (Toellner *et al.*, 1997). The direct beam passes through the second diamond anvil and is recorded by an avalanche photodiode detector (APD) for Mössbauer measurements in the time domain and as the zero-energy reference marker. The elastic and inelastic resonant excitation can be observed by the detection of the X-ray fluorescence (K_α and K_β) resulting from subsequent nuclear de-excitation.

The phonon DOS in the low-energy range provides an independent method for the determination of V_P and V_S at core pressures. Parabolic fitting of the low-energy end (<13 meV) of the DOS significantly below the van Hove singularity yields the Debye average phonon velocity (V_D) which is related to V_P and V_S by $3V_D^{-3} = V_P^{-3} + 2V_S^{-3}$. Accordingly, V_P and V_S can be solved. Our NRIXS results for V_P and V_S of ε-Fe up to 153 GPa are in excellent agreement with the extrapolated RXD data. More recently, additional data have been obtained in He pressure media to 50 GPa (Struzhkin, Mao *et al.*, 2004). The accuracy of V_P and V_S determinations by NRIXS has been confirmed by recent IXS (Antonangeli *et al.*, 2003) and impulsive scattering methods (Crowhurst *et al.*, 2003). The pressure dependence of the kinetic energy, zero-point energy, vibrational heat capacity, and vibrational entropy, can also be derived from the phonon DOS (Hu *et al.*, 1999). These properties further define other important geophysical parameters, such as the thermodynamic Debye temperature, Grüneisen parameter, and thermal expansivity. The results can be compared with vibrational spectra measured on Fe to above 150 GPa using Raman spectroscopies (Merkel, Goncharov *et al.*, 2000). Excellent agreement is found for the peak in the DOS identified as a van Hove singularity associated with the phonon measured by Raman spectroscopy (Hemley & Mao, 2001*a*; Merkel, Goncharov *et al.*, 2000).

Important advances have been made in extending these experiments for *in situ* high-*P*–*T* NRIXS techniques, including both resistive-heating (to 800 K) and laser-heating (>2000 K) methods. We have collaborated with XOR-CAT to build a laser-heating system for NRIXS. A Nd:YLF laser operating in continuous donut mode was used to heat a metallic sample of ^{57}Fe sample (>96% enrichment) from both sides of a diamond cell. Phonon velocities of iron were directly measured up to 58 GPa and 1500 K with NRIXS during laser heating (Fig. 8). Temperatures measured directly from the spectra using the principle of detailed balance (*i.e.* Stokes/anti-Stokes ratios of the inelastic phonon scattering) are in very good agreement with values determined from a Planck function fit to the thermal radiation, thus providing an independent method for primary temperature calibration under high-*P*–*T* conditions (Lin, Sturhahn *et al.*, 2004). The observed compressional and shear wave velocities of ε-Fe decrease with increasing temperature at high pressures, and a strong temperature effect on the linear sound-velocity–density relations (Birch's law) was found. The data provide detailed information on the intrinsic anharmonic properties of the material at high pressures and temperatures.

The technique can also be applied to other materials, including those containing ^{57}Fe as well as substances with other Mossbauer-active nuclei. Since NRIXS only detects phonon modes coupled with the active nuclei (*e.g.* ^{57}Fe), the DOS calculation for samples containing other elements is more complex. The Debye-like low-frequency dynamics measured for several Fe-containing compounds and alloys has been used to calculate the shear modulus and phonon velocities of the material (Hu *et al.*, 2003), although the accuracy of the approach needs to be tested on a broader range of materials and the theory extended. The technique has been

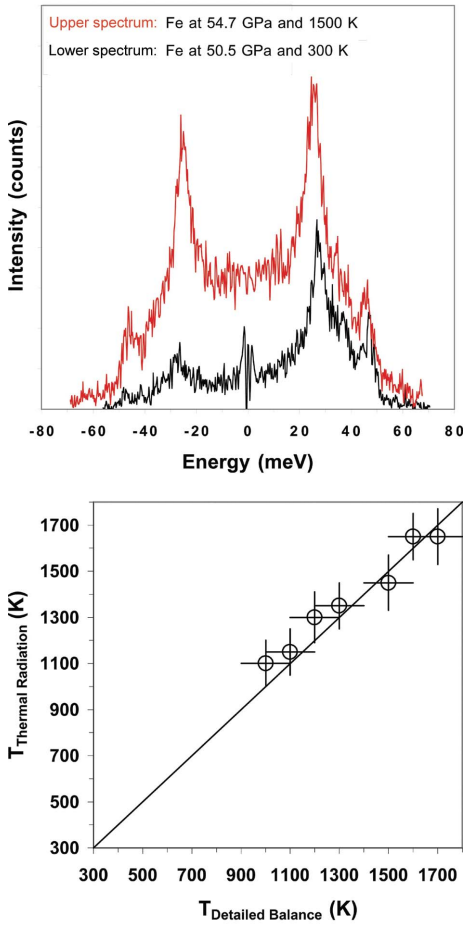

Figure 8
In situ high-*P*–*T* nuclear resonance inelastic scattering (NRIXS) measurements of ε-Fe. Top: spectra at 300 K and 1500 K at 50.5 and 54.7 GPa, respectively. Bottom: comparison of the temperature obtained from the thermal radiation (assuming a grey-body) and that obtained from the temperature dependence of the spectrum using detailed balance (Lin, Sturhahn *et al.*, 2004).

used to examine the high-pressure elasticity of FeO (Struzhkin *et al.*, 2001), FeH (Mao, Sturhahn *et al.*, 2004), and Fe–Si and Fe–Ni (Lin, Struzhkin *et al.*, 2003). The partial phonon DOS of FeO examined to 48 GPa (Struzhkin *et al.*, 2001) reveal the strong magnetoelastic coupling associated with the pressure-induced changes in FeO discussed above. NRIXS measurements on FeH to 40 GPa provided direct information on the low-frequency phonon DOS; because the hydrogen modes contribute little to the full DOS at low frequency, the measurements are believed to provide an accurate determination of the elasticity and vibrational thermodynamic properties (Mao, Sturhahn *et al.*, 2004). The technique can readily be extended to other Mossbauer-active nuclei (*e.g.* Sn and Kr).

As mentioned above, radiation scattering in the forward direction in these experiments provide the nuclear resonance forward-scattering (NRFS) spectrum. Measured in the time domain, hyperfine splittings can be reconstructed from the time-dependent intensity of a conventional Mössbauer spectrum. NRFS measurements thus yield valuable information on oxidation states, magnetism, and site occupancy of iron under extreme conditions (Jackson *et al.*, 2005; Lin *et al.*, 2005), thus complementing the X-ray emission measurements discussed above. Feasibility studies performed on FeO show a surprising persistence of the magnetic state at high temperature in the NiAs-type phase (Struzhkin *et al.*, 2005).

11. Inelastic X-ray scattering of electrons and phonons

Within the Born approximation, $S(q,\omega)$ is the space–time Fourier transform of the density correlation function and can be related to the electronic band structure and elementary excitations (such as phonons and plasmons) of the system. In comparison with light (optical) scattering, which probes only zero-momentum transfer transitions and is limited by the intrinsic energy gap of diamond windows (5 eV), inelastic X-ray scattering (IXS) spectroscopy covers wide length (momentum) as well as temporal (energy) scales. Recent work has demonstrated the feasibility of these techniques to studying the electronic structure of simple molecular systems. Measurements of the high-energy excitations of solid ^{4}He at 211 MPa showed the 23.2 eV exciton (Arms *et al.*, 2001), confirming and greatly extending the early IXS measurements at 61.5 MPa and 4.3 K (Schell *et al.*, 1995). Recent extensions of this work include measurements on the pressure dependence of the band gaps, excitons, and exciton binding energies of He and Ar (Schwoerer-Böhning *et al.*, 2005).

The unique quantum character of hydrogen imparts dramatic and distinct properties to the material at very high densities, including possibly novel superconductivity, superfluidity, and singular high energy density (Ashcroft, 2002). Owing to the absorption threshold of diamond near 5 eV, the hydrogen band gap could only be implied indirectly through measurements of refractive indices (Eggert *et al.*, 1990; Hemley *et al.*, 1991). Recent breakthroughs have enabled access to rich electronic information above 5 eV. The pressure dependencies of electronic spectra (*e.g.* band gap and excitons) above the diamond absorption threshold will be directly measured using IXS. An immediate priority will be to extend these measurements from the 10 GPa to the 100 GPa range. The pressure dependence of the low-energy excitons can be followed, which is important for possible condensation into the ground state (*e.g.* to form an excitonic insulator). High-pressure IXS can also probe the plasmon in the metallic state (both fluid and solid). The challenge will be to extend these measurements to much higher pressure to examine electronic structure (*e.g.* the band gap and nearby excitons) near predicted pressure-induced insulator–metal transitions in these systems.

The near-edge spectra can also be obtained by IXS but has been limited to ambient pressure studies. With recent advances in inelastic X-ray scattering spectroscopy, this limitation has been removed. The inelastic *K*-edge scattering of Be (111 eV), B (188 eV), C (284 eV), N (410 eV), and O (543 eV) under pressure has been observed. The technique has been used to probe bonding changes in the pressure-induced transition in graphite near 15 GPa (Mao, Mao, Eng *et al.*, 2003). Complemented by diffraction measurements on the

same sample, the results show that the high-pressure phase has an unusual mixture of σ and π bonding (Fig. 9). A transition in a graphitic h-BN has been the subject of a related study (Meng *et al.*, 2004). The experiment started with graphitic h-BN, the near-edge peaks corresponding to the π^* and σ^* bonding of B and N observed at low pressure. Above 12 GPa, the σ^* features grow at the expense of those associated with π^*, indicating that bonding changes are associated with the transition. The high-pressure phase is a framework superhard material. Most recently, application to the H_2O ice provided evidence for a new very low *P*–*T* phase (below 20 K and 0.25 GPa). High-pressure near *K*-edge spectroscopy of the second-row elements (Li to Ne) and near *L*-edge spectroscopy from Na to transition elements is now open to investigation. In particular, measurements of *K*-edge spectra of the various novel compounds formed at high pressure from simple molecular systems can now be performed.

High-pressure phonon dispersion measurements have been carried out for single-crystal Ar to 20 GPa (Occelli *et al.*, 2001) and polycrystalline ε-Fe to 110 GPa (Fiquet *et al.*, 2001). Pilot experiments have been carried out to study the high-pressure phonon dispersion of polycrystalline h.c.p.-Fe (IXS Beamline BL35XU SPring-8). The ESRF IXS study used a Si (8 8 8) monochromator with 6 meV resolution and 4–12 nm^{-1} Q range. We experimented with Si (8 8 8) and Si (11 11 11) having 6 and 1.5 meV resolution, respectively, at SPring-8 and found that, although the Si (8 8 8) gave four times more counts and yielded high-quality data at high Q, the high resolution of Si (11 11 11) is essential for constraining the low-Q data at 20–30 meV, which is crucial for determining velocities (near Q = 0) and testing the sine approximation. ε-Fe forms of a polycrystalline aggregate having strong preferred orientation with the *c* axis parallel to the diamond-cell compression axis (Wenk *et al.*, 2000). Previous phonon IXS experiments (Fiquet *et al.*, 2001) were performed with both incident and scattered X-rays near the diamond-cell axis, and the measurement was limited to phonons in the plane normal to the *c* axis which did not represent the aggregate V_P of a randomly oriented polycrystalline sample. We used panoramic diamond cells to study the phonon dispersion as a function of azimuth angle to the *c* axis, thus obtaining the complete elastic anisotropy directly (the elasticity tensor of a hexagonal system has cylindrical symmetry). Our initial experience with the ε-Fe sample at 46 GPa was quite encouraging, with high counting rate. With higher resolution, we could observe the orientation dependence of the phonon velocity and the deviation from the sine approximation. Large samples made possible by CVD diamonds, as described below, will be essential for efforts to extend IXS techniques to much higher pressure.

12. Synchrotron infrared spectroscopy

In this section we consider high-pressure applications of much longer wavelength synchrotron radiation, the near- to far-infrared. High-pressure synchrotron infrared spectroscopy has brought a new dimension to studies of materials at high densities. The development of synchrotron infrared spectroscopy as a whole is becoming a leading technique in synchrotron radiation research (Miller, 2005*b*). Infrared radiation at the VUV ring of the NSLS has up to $\sim 10^4$ times the brightness of a conventional thermal (lamp) source (Williams, 1990). Because of the significant enhancement in our ability to probe microscopic samples provided by this source, it is ideally suited to studies of materials under extreme pressures (Hemley, Goncharov *et al.*, 1998; Reffner *et al.*, 1994). When coupled with an FTIR interferometer and special microscopes for high-pressure cells, up to five orders of magnitude in sensitivity are gained relative to a grating system commonly used for high-pressure infrared measurements. This difference is not only one of spectral quality; it can be crucial for making experiments feasible, as in the case of far- and mid-IR reflectivity and absorption measurements at multi-megabar pressures or studies of mineral inclusions where sample sizes may be <5 μm or at the diffraction limit; experiments with a conventional source would typically require beams of >30 μm. Vibrational, electronic, and

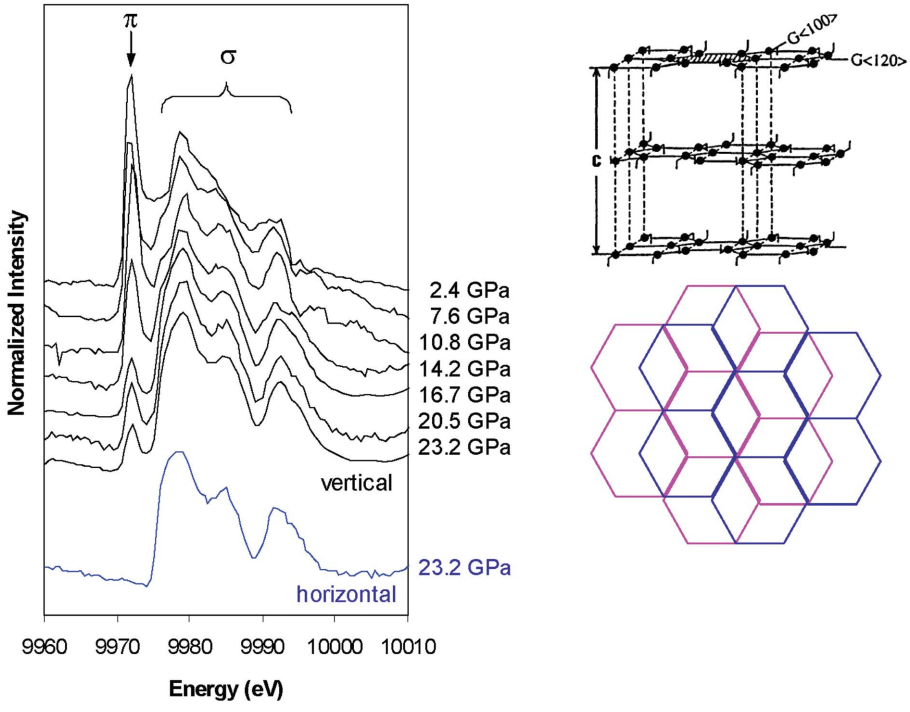

Figure 9
Inelastic scattering of graphite as a function of pressure across the transition near 16 GPa showing the changes in the *K*-edge structure indicative of changes in the relative amounts of σ and π bonding in the high-pressure phase. The topology of the graphite structure is shown on the right (Mao, Mao, Eng *et al.*, 2003).

magnetic excitations can be probed (Hemley, Goncharov *et al.*, 1998; Liu, Scott *et al.*, 2004). Enhanced flux can also be achieved with new infrared laser techniques (*e.g.* non-linear optical techniques and diode lasers), but the combination of very broad spectral distribution, ease of interfacing with a conventional FTIR instrument, and pulsed time structure provide important advantages of the synchrotron technique.

This technique led to a series of studies of materials at ultrahigh pressures, including the discovery of a number of unexpected phenomena in dense hydrogen, such as a striking intensity enhancement of the (formally forbidden) intramolecular stretching mode (Hemley, Mazin *et al.*, 1997), an interesting phase diagram (Hemley, Mazin *et al.*, 1997), and accurate bounds on metallization at megabar pressures (Hemley *et al.*, 1996). Important insights have been obtained from detailed studies of the pressure-induced transformations in molecular hydrogen at megabar pressures (*i.e.* phases I, II, and III) (Mao & Hemley, 1994). Direct measurements of electrical conductivity to 210 GPa show that solid hydrogen remains in an insulating state (at 300 K and below) to this pressure, consistent with the infrared study (Hemley *et al.*, 1996; see also Chen *et al.*, 1996). Additional measurements show stability of the molecule to >285 GPa (Fig. 10) (Goncharov *et al.*, 2001; Hemley & Mao, 1998).

Applications to other materials studied in the near- to mid-infrared include the following. Synchrotron infrared reflectivity spectra of H_2O to 210 GPa showed that the transition of ice to the long-sought, non-molecular, symmetric hydrogen-bonded structure occurs at 60 GPa (Goncharov *et al.*, 1996; Struzhkin *et al.*, 1997), consistent with lower-pressure conventional infrared measurements (Aoki *et al.*, 1996). In this work, extremely weak vibrational reflectance spectra were measured on a 20 µm sample within a metallic (reflecting) gasket, thereby demonstrating the power of the synchrotron technique. Multiple Fermi resonances (mode couplings) of the soft mode with other excitations before and after the transition to the non-molecular (ionic) phase were uncovered, and the isotope effect on the symmetrization transition was determined (*i.e.* for D_2O). Infrared measurements of H_2O in clathrates have been used to determine the stability field and physical properties of these potential fuel sources. Synchrotron infrared was also used to identify the ionic nature of the $NO^+NO_3^-$ phase discussed above (Somayazulu *et al.*, 2001).

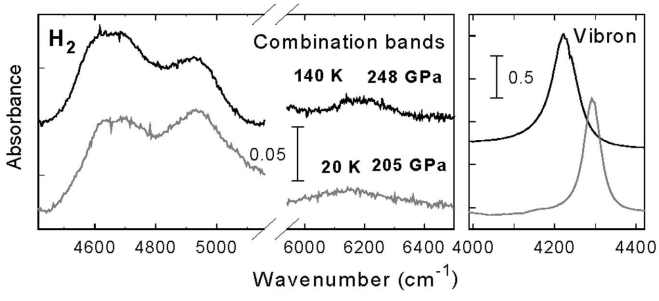

Figure 10
Synchrotron absorption spectra of hydrogen to 248 GPa and low temperature showing the persistence of the molecular state at these conditions (Goncharov *et al.*, 2001).

These measurements showed that the material forms a charge-transfer ('zwitterionic') phase, also examined by powder diffraction as discussed above. These infrared measurements have also shown that methane persists metastably to above 120 GPa at 300 K, in contrast to its breakdown under laser heating below 15 GPa (Benedetti *et al.*, 1999; Hemley, 2000). The technique has been instrumental in the discovery and characterization of new van der Waals compounds discussed above (*e.g.* Somayazulu *et al.*, 1997) as well as to identify the pressure-induced transitions in simple molecular systems such as nitrogen described above (Goncharov *et al.*, 2000; Gregoryanz *et al.*, 2001). More recently, a growing number of mid-IR studies of biological systems under pressure have been carried out, including bioceramic hydroxyapatite (Miller, 2005*a*) and mosaic pea virus (Li, 2005).

A particularly important new development has been the extension and improvement of far-IR measurements in diamond-anvil cells. For example, excellent measurements have been performed down to 20 cm^{-1} to identify the long-sought doming mode in heme compounds (Fig. 11) (Klug *et al.*, 2002). Interestingly, these experiments provided unique information that was not readily available from NRIXS measurements on related compounds, even at ambient pressure (Sage *et al.*, 2001). A high-pressure/low-temperature far-IR study ruled out a previously proposed isosymmetric phase transition in ice VIII (Klug *et al.*, 2004). A growing number of high-pressure far-IR investigations of minerals are being performed; these are particularly important for identifying phase-transformation mechanisms and thermodynamic properties at high pressure (Liu, Hu *et al.*, 2004; Liu *et al.*, 2002, 2003). Low-energy intraband (Drude) absorption diagnostic of metallization (see Hemley *et al.*, 1996) should provide useful comparison with the electronic IXS measurements described

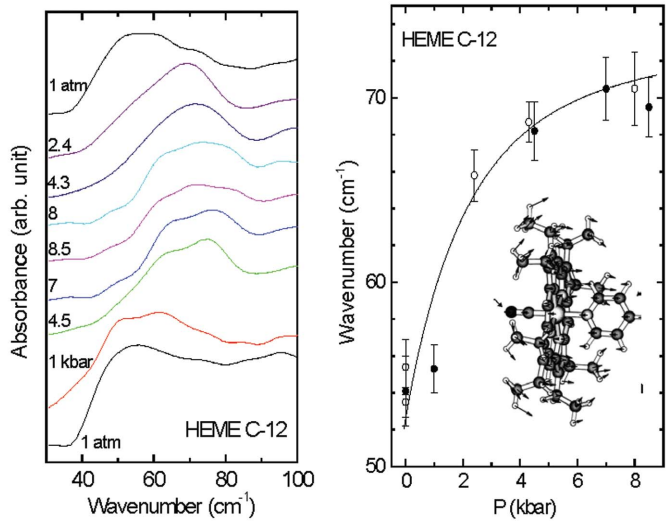

Figure 11
Synchrotron far-IR spectra of a model heme compound, CoFe(OEP)py. Left: spectra measured on a 500 µm × 500 µm sample in a diamond cell. Right: pressure dependence of the low-frequency (53 cm^{-1}) mode; the inset shows calculated atom displacements for the doming mode (Klug *et al.*, 2002).

above. The low-frequency modes are also important for constraining lattice symmetry and rotational states in the solid.

13. New materials for high-pressure research

Continued developments in high-pressure science depend critically upon advances in instrumentation. Among the most essential needs is the enlargement of sample volume without compromising the *P–T* range and accessibility for *in situ* measurements. This is essential for new classes of synchrotron experiments, particularly in the multimegabar range, including inelastic scattering which has low count rates with small samples, single-crystal diffraction where hydrostaticity in a large sample chamber is essential, and far-infrared spectroscopy where we need to maintain a large sample diamond to minimize optical diffraction effects. This means producing large gem anvils. One route is to employ other anvil materials that are more easily enlarged; this includes single-crystal SiC (moissanite), which has been used as an anvil material to reach pressures above 65 GPa (Xu & Mao, 2000; Xu *et al.*, 2002). Considerable progress has been made in scaling up this device with supported (belt-type) assemblies (Xu *et al.*, 2004). Moissanite also complements diamond for high-pressure infrared spectroscopy (Liu, Xu *et al.*, 2004).

During the past two years we have had considerable success producing single-crystal diamond by microwave plasma chemical vapor disposition (CVD; Fig. 12) (Yan *et al.*, 2002). X-ray experiments show that the hybrid high-*P–T*/CVD diamonds are at least as strong as the conventional diamonds we use, reaching at least 245 GPa based on X-ray diffraction of metal standards (Mao, Mao, Yan *et al.*, 2003). On high-*P–T* annealing these yellow diamonds become transparent. Moreover, we have found that all of these single crystals have very high fracture toughness relative to natural and synthetic diamond. More remarkable is the very high hardness of these same diamonds that have been subjected to high-*P–T* processing. This material has a Vickers hardness above 160 GPa (Yan *et al.*, 2004). In addition to its importance for static-pressure experiments, this new single-crystal material should enable new classes of shock-compression studies.

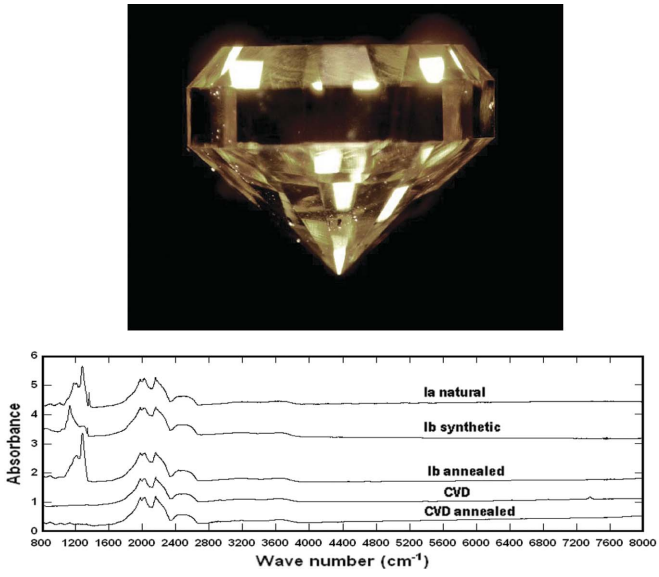

Figure 12
Top: photograph of an as-grown CVD single-crystal diamond polished in a brilliant cut. The crystal is 2.46 mm high; the top 0.45 mm (table) consists of a type-1b diamond substrate. Bottom: synchrotron infrared absorption spectra of CVD single-crystal diamond as compared with various natural diamond crystals.

Synchrotron radiation has been essential in characterizing this material, even as we aim to use it as the basis for new classes of high-pressure cells for synchrotron experiments. Moreover, infrared experiments have been carried out to characterize the defect structure and their changes on annealing (Fig. 12). The as-grown material contains hydrogen, as observed in the mid-IR and far-IR range. On annealing, the CH stretching modes sharpen and form a unique multiplet structure corresponding to distinct sites of residual hydrogen defects. In addition, this is coupled with a decrease in absorption (increased transparency) in the far-IR. These changes are also being correlated with X-ray topography of the as-grown and annealed material (Chen *et al.*, 2005). With further development, these single crystals could be used in other synchrotron applications, including monochromators and as substrates for detectors.

14. Conclusions

The combination of new high-pressure science and synchrotron radiation techniques has opened new vistas on the nature of materials as a function of density, with results that have a diversity of applications. The above examples illustrate that in this work the application of multiple techniques to the same materials under extreme conditions can shed important new light on the phenomena in question. Indeed, the power of an integrated approach is far greater than the sum of individual techniques; in newly developed beamlines, such integration allows multiple measurements to be performed on the same samples under extreme *P–T* conditions. In addition, a growing number of studies utilize the complementary roles of synchrotron X-ray and neutron scattering methods. Important developments in high-pressure cell design have occurred in the past two years: it has been shown that anvils can be enlarged as perfect single crystals by controlled chemical vapor deposition processes. This advance opens the prospect of a new generation of 'large volume' diamond-anvil cells giving orders-of-magnitude higher sample volumes at megabar pressures. This will then allow new experiments to be performed under these extreme conditions as well as extending many of the above techniques, including high-resolution inelastic X-ray scattering, to significantly higher pressures. Finally, the coupling of high-energy lasers and new coherent sources will make possible other new experiments such as high-*P–T* chemical dynamics in the time domain.

We thank numerous colleagues for their help in the work mentioned above, specifically D. Hausermann, J. F. Lin, J. Shu,

M. Somayazulu, E. Gregoryanz, Z. Liu, J. Hu, Q. Guo, M. Hu, P. Chow, W. Mao, S. Merkel, R. Wenk, J. Pehl, C. Kao, Y. Cai, C. Yan, Y. Song, X. Chen, Y. Chen, S. Gramsch, A. Goncharov, P. Eng, G. Shen, J. Badro, G. Fiquet, C. Sanloup, P. Gillet, M. Eremets, M. Santoro, L. Taylor, and M. Anand. Our X-ray measurements described above were carried out at sectors 16, 13, 11, and 3 of the APS; at beamlines X17C and X17B3 of the NSLS; and beamlines ID9 and ID30 of the ESRF. All infrared experiments were performed at beamline U2A of the NSLS. This research was supported by the NSF-DMR, NSF-EAR, DOE (BES and NNSA), NASA, and the W. M. Keck Foundation.

References

Akahama, Y., Kawamura, H., Häusermann, D., Hanfland, M. & Shimomura, O. (1995). *Phys. Rev. Lett.* **74**, 4690–4693.

Aleksandrov, I. V., Goncharov, A. F., Zisman, A. N. & Stishov, S. M. (1987). *Sov. Phys. JETP*, **66**, 384–390.

Alfè, D., Kresse, G. & Gillan, M. J. (2000). *Phys. Rev. B*, **61**, 132–142.

Anand, M., Taylor, L. A., Nazarav, M. A., Shu, J., Mao, H. K. & Hemley, R. J. (2004). *Proc. Nat. Acad. Sci.* **101**, 6847–6851.

Andrault, D., Fiquet, G., Guyot, F. & Hanfland, M. (1998). *Science*, **282**, 720–724.

Antonangeli, D., Occelli, F., Badro, J., Requardt, H., Fiquet, G. & Krisch, M. (2003). *Eos Trans. Am. Geophys. Union*, **T21F-04**.

Aoki, K., Yamawaki, H., Sakashita, M. & Fujihisa, H. (1996). *Phys. Rev. B*, **54**, 15673–15677.

Arms, D. A., Simmons, R. O., Schwoerer-Bohning, M., Macrander, A. T. & Graber, T. J. (2001). *Phys. Rev. Lett.* **87**, 156402-1–4.

Ashcroft, N. W. (2002). *High-Pressure Phenomena, Proceedings of the International School of Physics 'Enrico Fermi'*, edited by R. J. Hemley, G. L. Chiarotti, M. Bernasconi and L. Ulivi. pp. 151–195. Amsterdam: IOS Press.

Badro, J., Fiquet, G., Guyot, F., Rueff, J.-P., Struzhkin, V. V., Vanko, G. & Monaco, G. (2003). *Science*, **300**, 789–791.

Badro, J., Fiquet, G., Struzhkin, V. V., Somayazulu, M., Mao, H. K., Shen, G. & Le Bihan, T. (2002). *Phys. Rev. Lett.* **89**, 205504.

Badro, J., Rueff, J.-P., Vanko, G., Monaco, G., Fiquet, G. & Guyot, F. (2004). *Science*, **305**, 383–385.

Badro, J., Struzhkin, V. V., Shu, J., Hemley, R. J., Mao, H. K., Kao, C. C., Rueff, J. P. & Shen, G. (1999). *Phys. Rev. Lett.* **83**, 4101–4104.

Benedetti, L. R., Nguyen, J. H., Caldwell, W. A., Liu, H., Kruger, M. & Jeanloz, R. (1999). *Science*, **286**, 100–102.

Brazhkin, V. V. & Lyapin, A. G. (2000). *Phys. Uspekhi*, **43**, 493–508.

Caracas, R. & Cohen, R. E. (2005*a*). *Bull. Am. Phys. Soc.* In the press.

Caracas, R. & Cohen, R. E. (2005*b*). *Geophys. Res. Lett.* Submitted.

Carpenter, M. A., Hemley, R. J. & Mao, H. K. (2000). *J. Geophys. Res.* **105**, 10807–10816.

Chen, M., Shu, J., Mao, H. K., Xie, X. & Hemley, R. J. (2003). *Proc. Nat. Acad. Sci.* **100**, 14651–14654.

Chen, M., Shu, J., Xie, X. & Mao, H. K. (2003). *Geochim. Cosmochim. Acta*, **67**, 3937–3942.

Chen, N., Sterer, E. & Silvera, I. F. (1996). *Phys. Rev. Lett.* **76**, 1663–1666.

Chen, Y., Krasnicki, F., Yan, C., Mao, H. K. & Hemley, R. J. (2005). In preparation.

Chou, I. M., Sharma, A., Burruss, R. C., Shu, J., Mao, H. K., Hemley, R. J., Goncharov, A. F., Stern, L. A. & Kirby, S. H. (2000). *Proc. Nat. Acad. Sci.* **97**, 13484–13487.

Crowhurst, J. C., Zaug, J. M. & Goncharov, A. (2003). *Eos Trans. Am. Geophys. Union*, **T21F-03**.

Degtyareva, O., Gregoryanz, E., Somayazulu, M., Dera, P., Mao, H. K. & Hemley, R. J. (2005*a*). *Nature Mater.* **4**, 152–155.

Degtyareva, O., Gregoryanz, E., Somayazulu, M., Mao, H. K. & Hemley, R. J. (2005*b*). *Phys. Rev. B.* In the press.

Degtyareva, O., McMahon, M. I. & Nelmes, R. J. (2005). *High Pressure Res.* In the press.

Dera, P., Downs, R. T. & Prewitt, C. T. (2004). Editors. *Structure Determination by Single Crystal X-ray Diffraction at Megabar Pressures*, Argonne, IL, USA. 12–14 November 2004.

Dera, P., Prewitt, C. T., Boctor, N. & Hemley, R. J. (2002). *Am. Mineral.* **87**, 1018–1023.

Desgreniers, S., Vohra, Y. K. & Ruoff, A. L. (1990). *J. Phys. Chem.* **94**, 1117–1122.

Dewaele, A., Loubeyre, P. & Mezouar, M. (2002). *Phys. Rev. B*, **69**, 092106.

Dewaele, A., Loubeyre, P. & Mezouar, M. (2004). *Phys. Rev. B*, **70**, 094112.

Ding, Y., Degtyareva, O., Liu, H., Somayazulu, M., Meng, Y., Xu, J., Hemley, R. J., Mao, H. K. & Prewitt, C. T. (2005). In preparation.

Ding, Y., Mao, H. K., Liu, H., Shu, J., Xu, J., Hemley, R. J. & Häusermann, D. (2005). In preparation.

Ding, Y., Xu, J., Prewitt, C. T., Hemley, R. J., Mao, H. K., Cowan, J. A., Zhang, J., Aian, J., Vogel, S. C. & Zhao, Y. (2005). *Appl. Phys. Lett.* In the press.

Duffy, T. S. & Ahrens, T. J. (1995). *J. Geophys. Res.* **100**, 529–542.

Duffy, T. S., Hemley, R. J. & Mao, H. K. (1995). *Phys. Rev. Lett.* **74**, 1371–1374.

Duffy, T. S., Shen, G., Heinz, D. L., Shu, J., Ma, Y., Hemley, R. J. & Mao, H. K. (1999). *Phys. Rev. B*, **60**, 15063–15073.

Duffy, T. S., Shen, G., Shu, J., Mao, H. K., Hemley, R. J. & Singh, A. K. (1999). *J. Appl. Phys.* **86**, 6729–6736.

Eggert, J. H., Geottel, K. A. & Silvera, I. F. (1990). *Europhys. Lett.* **11**, 775–781.

Eggert, J. H., Weck, G., Loubeyre, P. & Mezouar, M. (2002). *Phys. Rev. B*, **65**, 174105.

Eremets, M. I., Gavriliuk, A. G., Serebryanaya, N. R., Trojan, I. A., Dzivenko, D. A., Boehler, R., Mao, H. K. & Hemley, R. J. (2004). *J. Chem. Phys.* **121**, 11296.

Eremets, M. I., Gavriliuk, A. G., Trojan, I. A., Dzivenko, D. A. & Boehler, R. (2004). *Nature Mater.* **3**, 558–563.

Eremets, M. I., Hemley, R. J., Mao, H. K. & Gregoryanz, E. (2001). *Nature (London)*, **411**, 170–174.

Fei, Y., Li, J., Hirose, K., Minarik, W., Orman, J. V., Sanloup, C., van Westrenen, W., Komabayashi, T. & Funakoshi, K. (2004). *Phys. Earth Planet. Inter.* **143/144**, 516–526.

Fiquet, G., Andrault, D., Dewaele, A., Charpin, T., Kunz, M. & Haüsermann, D. (1998). *Phys. Earth Planet. Inter.* **105**, 21–31.

Fiquet, G., Andrault, D., Itie, J. P., Gillet, P. & Richet, P. (1996). *Phys. Earth Planet. Inter.* **95**, 1–17.

Fiquet, G., Badro, J., Guyot, F., Requardt, H. & Krisch, M. (2001). *Science*, **291**, 468–471.

Gannarelli, C. M. S., Alfè, D. & Gillan, M. J. (2003). *Phys. Earth Planet. Inter.* **139**, 243–253.

Goncharov, A. F., Gregoryanz, E., Hemley, R. J. & Mao, H. K. (2001). *Proc. Nat. Acad. Sci.* **98**, 14234–14237.

Goncharov, A. F., Gregoryanz, E., Hemley, R. J. & Mao, H. K. (2003). *Phys. Rev. B*, **68**, 100102.

Goncharov, A. F., Gregoryanz, E., Mao, H. K., Liu, Z. & Hemley, R. J. (2000). *Phys. Rev. Lett.* **85**, 1262–1265.

Goncharov, A. F., Struzhkin, V. V., Mao, H. K. & Hemley, R. J. (2005). *Phys. Rev. B.* In the press.

Goncharov, A. F., Struzhkin, V. V., Somayazulu, M., Hemley, R. J. & Mao, H. K. (1996). *Science*, **273**, 218–220.

Gorelli, F., Giordano, V. M., Salvi, P. R. & Bini, R. (2004). *Phys. Rev. Lett.* **93**, 205503.

Gorelli, F. A., Ulivi, L., Santoro, M. & Bini, R. (1999). *Phys. Rev. B*, **60**, 6179–6182.
Gregoryanz, E., Degtyareva, O., Somayazulu, M., Mao, H. K. & Hemley, R. J. (2005). To be published.
Gregoryanz, E., Goncharov, A. F., Hemley, R. J. & Mao, H. K. (2001). *Phys. Rev. B*, **64**, 052103.
Gregoryanz, E., Goncharov, A. F., Hemley, R. J., Mao, H. K., Somayazulu, M. & Shen, G. (2002). *Phys. Rev. B*, **66**, 224108.
Gregoryanz, E., Sanloup, C., Somayazulu, M., Badro, J., Fiquet, G., Mao, H. K. & Hemley, R. J. (2004). *Nature Mater.* **3**, 294–297.
Guthrie, M., Tulk, C. A., Benmore, C. J., Xu, J., Yarger, J. L., Klug, D. D., Tse, J. S., Mao, H. K. & Hemley, R. J. (2004). *Phys. Rev. Lett.* **93**, 115502.
Hanfland, M., Syassen, K., Christensen, N. E. & Novikov, D. L. (2000). *Nature (London)*, **408**, 174–178.
Hemley, R. J. (2000). *Ann. Rev. Phys. Chem.* **51**, 763–800.
Hemley, R. J., Chiarotti, G., Bernasconi, M. & Ulivi, L. (2002). Editors. *High-Pressure Phenomena, Proceedings of the International School of Physics 'Enrico Fermi' Course CXLVII.* Amsterdam: IOS Press.
Hemley, R. J., Goncharov, A. F., Lu, R., Li, M., Struzhkin, V. V. & Mao, H. K. (1998). *II Nuovo Cimento D*, **20**, 539.
Hemley, R. J., Hanfland, M. & Mao, H. K. (1991). *Nature (London)*, **350**, 488–491.
Hemley, R. J. & Mao, H. K. (1998). *J. Phys. Condens. Matter*, **10**, 11157–11167.
Hemley, R. J. & Mao, H. K. (2001*a*). *Int. Geol. Rev.* **43**, 1–30.
Hemley, R. J. & Mao, H. K. (2001*b*). *J. Low Temp. Phys.* **122**, 331–344.
Hemley, R. J. & Mao, H. K. (2002). *High Pressure Phenomena, Proceedings of the International School of Physics 'Enrico Fermi' Course CXLVII*, edited by R. J. Hemley, G. L. Chiarotti, M. Bernasconi and L. Ulivi. pp. 3–40. Amsterdam: IOS Press.
Hemley, R. J., Mao, H. K. & Cohen, R. E. (1998). *Ultrahigh-Pressure Mineralogy*, *Rev. Min.*, Vol 37, edited by R. J. Hemley, pp. 591–638. Washington, DC: Mineralogical Society of America.
Hemley, R. J., Mao, H. K., Finger, L. W., Jephcoat, A. P., Hazen, R. M. & Zha, C. S. (1990). *Phys. Rev. B*, **42**, 6458–6470.
Hemley, R. J., Mao, H. K., Goncharov, A. F., Hanfland, M. & Struzhkin, V. V. (1996). *Phys. Rev. Lett.* **76**, 1667–1670.
Hemley, R. J., Mao, H. K., Shen, G., Badro, J., Gillet, P., Hanfland, M. & Hausermann, D. (1997). *Science*, **276**, 1242–1245.
Hemley, R. J., Mazin, I. I., Goncharov, A. F. & Mao, H. K. (1997). *Europhys. Lett.* **37**, 403–407.
Hemley, R. J., Shu, J., Carpenter, M. A., Hu, J., Mao, H. K. & Kingma, K. J. (2000). *Solid State Commun.* **114**, 527–532.
Hemley, R. J., Zha, C. S., Jephcoat, A. P., Mao, H. K., Finger, L. W. & Cox, D. E. (1989). *Phys. Rev. B*, **39**, 11820–11827.
Hirose, K., Fei, Y., Ma, Y. & Mao, H. K. (1999). *Nature (London)*, **397**, 53–56.
Holt, M., Wu, Z., Hong, H., Zschack, P., Jemian, P., Tischler, J., Chen, H. & Chiang, T.-C. (1999). *Phys. Rev. Lett.* **83**, 3318–3321.
Hu, M. Y., Sturhahn, W., Toellner, T. S., Hession, P. M., Sutter, J. P. & Alp, E. E. (1999). *Nucl. Instrum. Methods Phys. Res. A*, **428**, 551–555.
Hu, M. Y., Sturhahn, W., Toellner, T. S., Mannheim, P. D., Brown, D. E., Zhao, J. & Alp, E. E. (2003). *Phys. Rev. B*, **67**, 094304.
Iitaka, T., Hirose, K., Kawamura, K. & Murakami, M. (2004). *Nature (London)*, **430**, 442–445.
Iota, V., Park, J. H. & Yoo, C. S. (2004). *Phys. Rev. B*, **69**, 004106.
Jackson, J. M., Struhahn, W., Shen, G., Zhao, J., Hu, M., Errandonea, D., Bass, J. D. & Fei, Y. (2005). *Am. Mineral.* In the press.
Jacobsen, S., Lin, J., Dera, P., Shen, G., Prakapenka, V., Mao, H. K. & Hemley, R. J. (2004). *Structure Determination by Single Crystal X-ray Diffraction at Megabar Pressures*, Argonne, IL, USA, 12–14 November 2004, p. 18 (abstract).
Jeanloz, R. & Kavner, A. (1996). *Philos. Trans. R. Soc. Lond. A*, **354**, 1279–1305.
Karato, S.-I., Forte, A. M., Liebermann, R. C., Masters, G. & Stixrude, L. (2000). Editors. *Earth's Deep Interior: Mineral Physics and Tomography from the Atomic to the Global Scale.* Washington, DC: American Geophysical Union.
Katayama, Y., Mizutani, T., Utsumi, W., Shimomura, O., Yamakata, M. & Funakoshi, K. (2000). *Nature (London)*, **403**, 170–173.
Katrusiak, A. & McMillan, P. F. (2004). Editors. *Proceedings of the Erice School of High-Pressure Crystallography.* Bristol: IUCr/IOP.
Kavner, A. (2003). *Earth Planet. Sci. Lett.* **214**, 645–654.
Kavner, A. & Duffy, T. S. (2001). *Geophy. Res. Lett.* **28**, 2691–2694.
Kawamura, H., Akahama, Y., Umemoto, S., Takemura, K., Ohishi, Y. & Shimomura, O. (2001). *Solid State Commun.* **119**, 29–32.
Kingma, K. J., Cohen, R. E., Hemley, R. J. & Mao, H. K. (1995). *Nature (London)*, **374**, 243–245.
Kingma, K. J., Mao, H. K. & Hemley, R. J. (1996). *High Press. Res.* **14**, 363–374.
Klug, D. D., Tse, J. S., Liu, Z., Gonze, X. & Hemley, R. J. (2004). *Phys. Rev. B*, **70**, 144113.
Klug, D. D., Zgierski, M. Z., Tse, J. S., Liu, Z., Kincaid, J. R., Czarnecki, K. & Hemley, R. J. (2002). *Proc. Nat. Acad. Sci.* **99**, 12526–12530.
Kunc, K., Loa, I. & Syassen, K. (2003). *Phys. Rev. B*, **68**, 094107.
Li, J., Struzhkin, V. V., Mao, H. K., Shu, J., Hemley, R. J., Fei, Y., Mysen, B., Dera, P., Prakapenka, V. & Shen, G. (2004). *Proc. Nat. Acad. Sci.* **101**, 14027–14030.
Li, T. (2005). In preparation.
Lin, J.-F., Degtyareva, O., Prewitt, C. T., Dera, P., Sata, N., Gregoryanz, E., Mao, H. K. & Hemley, R. J. (2004). *Nature Mater.* **3**, 389–393.
Lin, J. F., Fei, Y., Sturhahn, W., Zhao, J., Mao, H. K. & Hemley, R. J. (2004). *Earth Planet Sci. Lett.* In the press.
Lin, J. F., Heinz, D. L., Mao, H. K., Hemley, R. J., Devine, J. M., Li, J. & Shen, G. (2003). *Proc. Nat. Acad. Sci.* **100**, 4405–4408.
Lin, J.-F., Struzhkin, V. V., Jacobsen, S., Hu, M. Y., Liu, H., Chow, P., Liu, H., Mao, H. K. & Hemley, R. J. (2004). *Eos Trans. AGU Fall Meet. Suppl.* **85**, Abstract MR14A-06.
Lin, J. F., Struzhkin, V. V., Mao, H. K., Hemley, R. J., Chow, P., Hu, M. & Li, J. (2004). *Phys. Rev. B*, **70**, 212405.
Lin, J. F., Struzhkin, V. V., Sturhahn, W., Huang, E., Zhao, J., Hu, M., Alp, E., Mao, H. K., Boctor, N. & Hemley, R. J. (2003). *Geophys. Res. Lett* **30**, 2112–2115.
Lin, J. F., Sturhahn, W., Zhao, J., Shen, G., Mao, H. K. & Hemley, R. J. (2004). *Geophys. Res. Lett.* **31**, L14611.
Lin, J.-F., Sturhahn, W., Zhao, J., Shen, G., Mao, H. K. & Hemley, R. J. (2005). *Frontiers in High-Pressure Research*, edited by J. Chen, Y. Wang, T. Duffy, G. Shen and L. Dobrzhinetskaya. In the press.
Liu, H., Hu, J., Xu, J., Liu, Z., Shu, J., Mao, H. K. & Chen, J. (2004). *Phys. Chem. Miner.* **31**, 240–246.
Liu, Z., Hu, J., Yang, H., Mao, H. K. & Hemley, R. J. (2002). *J. Phys. Condens. Matter*, **14**, 10641–10646.
Liu, Z., Lager, G. A., Hemley, R. J. & Ross, N. L. (2003). *Am. Mineral.* **88**, 1412–1415.
Liu, Z., Xu, J., Scott, H., Williams, Q., Mao, H. K. & Hemley, R. J. (2004). *Rev. Sci. Instrum.* In the press.
Lorenzana, H. E., Lipp, M. J. & Evans, W. J. (2002). *High Press. Res.* **22**, 5–8.
Loubeyre, P. (2003). Private communication.
Loubeyre, P., LeToullec, R., Hausermann, D., Hanfland, M., Hemley, R. J., Mao, H. K. & Finger, L. W. (1996). *Nature (London)*, **383**, 702–704.
Loubeyre, P., Letoullec, R., Pinceaux, J. P., Mao, H. K., Hu, J. & Hemley, R. J. (1993). *Phys. Rev. Lett.* **71**, 2272–2275.
Loubeyre, P., LeToullec, R., Wolanin, E., Hanfland, M. & Hausermann, D. (1999). *Nature (London)*, **397**, 503–506.
Ma, Y., Somayazulu, M., Mao, H. K., Shu, J., Shen, G. & Hemley, R. J. (2004). *Phys. Earth Planet. Inter.* **143/144**, 455–467.
McMahan, A. K. & LeSar, R. (1985). *Phys. Rev. Lett.* **54**, 1929–1932.

McMahon, M. I., Degtyareva, O. & Nelmes, R. J. (2000). *Phys. Rev. Lett.* **85**, 4896–4899.
McMahon, M. I., Nelmes, R. J. & Rekhi, S. (2001). *Phys. Rev. Lett.* **87**, 255502.
McMillan, P. F. (2002). *Nature Mater.* **1**, 19–25.
Mailhiot, C., Yang, L. H. & McMahan, A. K. (1992). *Phys. Rev. B*, **46**, 14419–14435.
Manga, M. & Jeanloz, R. (1997). *J. Geophys. Res.* **102**, 2999–3008.
Mao, H. K. (2003). *Eos Trans. AGU Fall Meet. Suppl.* **84**, Abstract V41B-02.
Mao, H. K., Bell, P. M., Shaner, J. W. & Steinberg, D. J. (1978). *J. Appl. Phys.* **49**, 3276–3283.
Mao, H. K. & Hemley, R. J. (1994). *Rev. Mod. Phys.* **66**, 671–692.
Mao, H. K., Hemley, R. J., Wu, Y., Jephcoat, A. P., Finger, L. W., Zha, C. S. & Bassett, W. A. (1988). *Phys. Rev. Lett.* **60**, 2649–2652.
Mao, H. K., Jephcoat, A. P., Hemley, R. J., Finger, L. W., Zha, C. S., Hazen, R. M. & Cox, D. E. (1988). *Science*, **239**, 1131–1134.
Mao, H. K., Shen, G., Hemley, R. J. & Duffy, T. S. (1998). *Properties of Earth and Planetary Materials at High Pressure and Temperature*, edited by M. H. Manghnani & T. Yagi. pp. 27–34. Washington, DC: AGU.
Mao, H. K., Shu, J., Fei, Y., Hu, J. & Hemley, R. J. (1996). *Phys. Earth Planet. Inter.* **96**, 135–145.
Mao, H. K., Shu, J., Shen, G., Hemley, R. J., Li, B. & Singh, A. K. (1998). *Nature (London)*, **396**, 741–743; Erratum: *Nature (London)*, (1999), **399**, 280.
Mao, H. K., Xu, J. & Bell, P. M. (1986). *J. Geophys. Res.* **91**, 4673–4676.
Mao, H. K., Xu, J., Struzhkin, V. V., Shu, J., Hemley, R. J., Sturhahn, W., Hu, M. Y., Alp, E. E., Vocadlo, L., Alfè, D., Price, G. D., Gillan, M. J., Schwoerer-Böhning, M., Häusermann, D., Eng, P., Shen, G., Gieffer, H., Lübbers, R. & Wortmann, G. (2001). *Science*, **292**, 914–916.
Mao, W. L. & Mao, H. K. (2004). *Proc. Nat. Acad. Sci.* **101**, 708–710.
Mao, W. L., Mao, H.-K., Eng, P. J., Trainor, T. P., Newville, M., Kao, C.-C., Heinz, D. L., Shu, J., Meng, Y. & Hemley, R. J. (2003). *Science*, **302**, 425–427.
Mao, W. L., Mao, H. K., Goncharov, A. F., Struzhkin, V. V., Guo, Q., Hu, J., Shu, J., Hemley, R. J., Somayazulu, M. & Zhao, Y. (2002). *Science*, **297**, 2247–2249.
Mao, W. L., Mao, H. K., Yan, C.S., Shu, J., Hu, J. & Hemley, R. J. (2003). *Appl. Phys. Lett.* **83**, 5190–5192.
Mao, W. L., Shen, G., Prakapenka, V. B., Meng, Y., Campbell, A. L., Heinz, D. L., Shu, J., Hemley, R. J. & Mao, H. K. (2004). *Proc. Nat. Acad. Sci.* **101**, 15867–15869.
Mao, W. L., Sturhahn, W., Heinz, D. L., Mao, H. K., Shu, J. & Hemley, R. J. (2004). *Geophys. Res. Lett.* **31**, L15618.
Martin, R. M. & Needs, R. (1986). *Phys. Rev. B*, **34**, 5082–5092.
Matthies, S., Merkel, S., Wenk, H. R., Hemley, R. J. & Mao, H. K. (2001). *Earth Planet Sci. Lett.* **194**, 201–212.
Mattson, W. D., Sanchez-Portal, D., Chiesa, S. & Martin, R. M. (2004). *Phys. Rev. Lett.* **93**, 125501.
Meade, C., Hemley, R. J. & Mao, H. K. (1992). *Phys. Rev. Lett.* **69**, 1387–1390.
Meng, Y., Mao, H. K., Eng, P. J., Trainor, T. P., Newville, M., Hu, M. Y., Kao, C., Shu, J., Hausermann, D. & Hemley, R. J. (2004). *Nature Mater.* **3**, 111–114.
Merkel, S., Goncharov, A. F., Mao, H. K., Gillet, P. & Hemley, R. J. (2000). *Science*, **288**, 1626–1629.
Merkel, S., Hemley, R. J. & Mao, H. K. (1999). *Appl. Phys. Lett.* **74**, 656–658.
Merkel, S., Hemley, R. J., Mao, H. K. & Teter, D. M. (2000). *Science and Technology of High Pressure*, edited by M. H. Manghnani, W. J. Nellis & M. Nicol. pp. 68–73. Hyderabad, India: Universities Press.
Merkel, S., Wenk, H. R., Badro, J., Montagnac, G., Gillet, P., Mao, H. K. & Hemley, R. J. (2003). *Earth Planet. Sci. Lett.* **209**, 351–360.
Merkel, S., Wenk, H.-R., Gillet, P., Mao, H. K. & Hemley, R. J. (2004). *Phys. Earth Planet. Inter.* **145**, 239–251.
Merkel, S., Wenk, H. R., Shu, J., Shen, G., Gillet, P., Mao, H. K. & Hemley, R. J. (2002). *J. Geophys. Res.* **107**, 2271.
Merkel, S., Yagi, T., Miyajima, N., Wenk, R., Mao, H. K. & Hemley, R. J. (2004). *Eos Trans. AGU Fall Meet. Suppl.* In the press.
Miller, L. (2005*a*). To be published.
Miller, L. (2005*b*). *Rev. Sci. Instrum.* In the press.
Murakami, M., Hirose, K., Kawamura, K., Sata, N. & Ohishi, Y. (2004). *Science*, **304**, 855–858.
Neaton, J. B. & Ashcroft, N. W. (1999). *Nature (London)*, **400**, 141–144.
Neaton, J. B. & Ashcroft, N. W. (2001). *Phys. Rev. Lett.* **86**, 2830–2833.
Nguyen, J. H. & Holmes, N. C. (2004). *Nature (London)*, **427**, 339–342.
Occelli, F., Krisch, M., Loubeyre, P., Sette, F., Le Toullec, R., Masciovecchio, C. & Rueff, J.-P. (2001). *Phys. Rev. B*, **63**, 224306.
Oganov, A. R. & Ono, S. (2004). *Nature (London)*, **430**, 445–448.
Pasternak, M. P., Rozenberg, G. K., Machavariani, G. Y., Naaman, O., Taylor, R. D. & Jeanloz, R. (1999). *Phys. Rev. Lett.* **82**, 4663–4666.
Pasternak, M. P., Taylor, R. D., Jeanloz, R., Li, X., Nguyen, J. H. & McCammon, C. A. (1997). *Phys. Rev. Lett.* **79**, 5046–5049.
Pehl, J., Wenk, H., Devine, J. M., Shen, G., Prakapenka, V., Mao, H. K., Hemley, R. J. & Merkel, S. (2003). *Eos Trans. AGU Fall Meeting Suppl. Abstract T22D-08*, **84** (46).
Poirier, J. P. & Price, G. D. (1999). *Phys. Earth Planet. Inter.* **110**, 147–156.
Reffner, J., Carr, G. L., Sutton, S., Hemley, R. J. & Williams, G. P. (1994). *Synchrotron Rad. News*, **7**, 30.
Rueff, J. P., Kao, C. C., Struzhkin, V. V., Badro, J., Shu, J. F., Hemley, R. J. & Mao, H. K. (1999). *Phys. Rev. Lett.* **82**, 3284–3287.
Ruoff, A. L., Lincoln, R. C. & Chen, Y. C. (1973). *J. Phys. D*, **6**, 1295–1306.
Sage, J. T., Durbin, S. M., Sturhahn, W., Wharton, D. C., Champion, P. M., Hession, P., Sutter, J. & Alp, E. E. (2001). *Phys. Rev. Lett.* **86**, 4966–4969.
Sanloup, C., Guyot, F., Gillet, P., Fiquet, G., Hemley, R. J., Mezouar, M. & Martinez, I. (2000*a*). *Europhys. Lett.* **52**, 151–157.
Sanloup, C., Guyot, F., Gillet, P., Fiquet, G., Mezouar, M. & Martinez, I. (2000*b*). *Geophys. Res. Lett.* **27**, 811–814.
Sanloup, C., Mao, H. K. & Hemley, R. J. (2002). *Proc. Nat. Acad. Sci.* **99**, 25–28.
Santoro, M., Gregoryanz, E., Mao, H. K. & Hemley, R. J. (2004). *Phys. Rev. Lett.*
Santoro, M., Lin, J.-F., Mao, H. K. & Hemley, R. J. (2004). *J. Chem. Phys.* **121**, 2780–2787.
Schell, N., Simmons, R. O., Kaprolat, A., Schülke, W. & Burkel, E. (1995). *Phys. Rev. Lett.* **74**, 2535–2538.
Schweika, W., Hoser, A., Martin, M. & Carlsson, A. E. (1995). *Physica B*, **213**, 570–572.
Schwoerer-Böhning, M., Macrander, A. T., Mao, H. K. & Gog, T. (2005). To be published.
Seto, M., Yoda, Y., Kikuta, S., Zhang, X. W. & Ando, M. (1995). *Phys. Rev. Lett.* **74**, 3828–3831.
Shen, G. & Heinz, D. L. (1998). *Ultrahigh-Pressure Mineralogy: Physics and Chemistry of the Earth's Deep Interior*, edited by R. J. Hemley, pp. 369–396. Washington, DC: Mineralogical Society of America.
Shen, G., Prakapenka, V. B., Rivers, M. L. & Sutton, S. R. (2003). *Rev. Sci. Instrum.* **74**, 3021–3026.
Shen, G., Prakapenka, V. B., Rivers, M. L. & Sutton, S. R. (2004). *Phys. Rev. Lett.* **92**, 185701.
Shen, G., Rivers, M. L., Wang, Y. & Sutton, S. R. (2000). *Rev. Sci. Instrum.* **72**, 1273–1282.
Shen, G., Sata, N., Newville, M., Rivers, M. L. & Sutton, S. R. (2002). *Appl. Phys. Lett.* **81**, 1411–1413.
Shieh, S. R., Duffy, T. S. & Li, B. (2002). *Phys. Rev. Lett.* **89**, 255507.
Shieh, S. R., Mao, H. K., Hemley, R. J. & Ming, L. C. (2000). *Earth Planet. Sci. Lett.* **177**, 69–80.
Shieh, S. R., Mao, H. K., Konzett, J. & Hemley, R. J. (2000). *Am. Mineral.* **85**, 765–769.

Shieh, S. R., Ming, L. C., Mao, H. K. & Hemley, R. J. (1998). *Earth Planet. Sci. Lett.* **159**, 13–23.
Shimizu, K., Suhara, K., Ikumo, M., Eremets, M. I. & Amaya, K. (1998). *Nature (London)*, **393**, 767–769.
Shu, J., Mao, H. K., Hu, J., Fei, Y. & Hemley, R. J. (1998). *Neues Jahr. Mineral.* **172**, 309–323.
Sihachakr, D. & Loubeyre, P. (2004). *Phys. Rev. B*, **70**, 134105.
Singh, A. K., Mao, H. K., Shu, J. & Hemley, R. J. (1998). *Phys. Rev. Lett.* **80**, 2157–2160.
Sobolev, N. V., Fursenko, B. A., Goryainov, S. V., Shu, J., Hemley, R. J., Mao, H. K. & Boyd, F. R. (2000). *Proc. Nat. Acad. Sci.* **97**, 11875–11879.
Somayazulu, M., Madduri, A., Goncharov, A. F., Tschauner, O., McMillan, P. F., Mao, H. K. & Hemley, R. J. (2001). *Phys. Rev. Lett.* **87**, 135504.
Somayazulu, M. S., Hemley, R. J., Goncharov, A. F., Mao, H. K. & Finger, L. W. (1997). *Eur. J. Solid State Inorg. Chem.* **34**, 705–713.
Song, Y., Somayazulu, M., Mao, H. K., Hemley, R. J. & Herschbach, D. R. (2003). *J. Chem. Phys.* **118**, 8350–8356.
Speziale, S., Zha, C. S., Duffy, T. S., Hemley, R. J. & Mao, H. K. (2001). *J. Geophys. Res.* **106**, 515–528.
Steinle-Neumann, G., Stixrude, L., Cohen, R. E. & Gülseren, O. (2001). *Nature (London)*, **413**, 57–60.
Struzhkin, V. V., Goncharov, A. F., Hemley, R. J. & Mao, H. K. (1997). *Phys. Rev. Lett.* **78**, 4446–4449.
Struzhkin, V. V., Hemley, R. J. & Mao, H. K. (2004). *J. Phys. Condens. Matter*, **16**, 1–16.
Struzhkin, V. V., Lin, J. F., Sturhahn, W., Zhao, J., Mao, H. K., Hemley, R. J. & Boctor, N. (2005). In preparation.
Struzhkin, V. V., Mao, H. K., Hu, J., Schwoerer-Böhning, M., Shu, J., Hemley, R. J., Sturhahn, W., Hu, M. Y., Alp, E. E., Eng, P. & Shen, G. (2001). *Phys. Rev. Lett.* **87**, 255501.
Struzhkin, V. V., Mao, H. K., Mao, W. L., Hemley, R. J., Sturhahn, W., Alp, E. E., L'Abbe, C., Hu, M. Y. & Errandonea, D. (2004). *Hyperfine Interact.* **153**, 3–15.
Sturhahn, W., Toellner, T. S., Alp, E. E., Zhang, X. W., Ando, M., Yoda, Y., Kikuta, S., Seto, M., Kimball, C. W. & Dabrowski, B. (1995). *Phys. Rev. Lett.* **74**, 3832–3835.
Takemura, K., Christensen, N. E., Novikov, D. L., Syassen, K., Schwarz, U. & Hanfland, M. (2000). *Phys. Rev. B*, **61**, 14399.
Tamura, N., Celestre, R. S., MacDowell, A. A., Padmore, H. A., Spolenak, R., Valek, B. C., Chang, N. M., Manceau, A. & Patel, J. R. (2002). *Rev. Sci. Instrum.* **73**, 1369–1372.
Tamura, N., MacDowell, A. A., Celestre, R. S., Padmore, H. A., Valek, B. C., Bravman, J. C., Spolenak, R., Brown, W. L., Marieb, T., Fujimoto, H., Batterman, B. W. & Patel, J. R. (2002). *Appl. Phys. Lett.* **80**, 3724–3727.
Terasaki, H., Kato, T., Urakawa, S., Funakoshi, K., Sato, K., Suzuki, A. & Okada, T. (2002). *Geophys. Res. Lett.* **29**, 1227.
Toellner, T. S., Hu, M. Y., Sturhahn, W., Quast, K. & Alp, E. E. (1997). *Appl. Phys. Lett.* **71**, 2112–2114.
Tschauner, O., Mao, H. K. & Hemley, R. J. (2001). *Phys. Rev. Lett.* **87**, 075701.
Tsuchiya, T., Tsuchiya, J., Umemoto, K. & Wentzcovitch, R. M. (2004*a*). *Geophys. Res. Lett.* **31**, 4603.
Tsuchiya, T., Tsuchiya, J., Umemoto, K. & Wentzcovitch, R. M. (2004*b*). *Earth Planet. Sci. Lett.* **224**, 241.
Utsumi, W., Weidner, D. J. & Liebermann, R. C. (1998). *Properties of Earth and Planetary Materials at High Pressures and Temperatures*, edited by M. H. Manghnani and T. Yagi, pp. 327–333. Washington, DC: American Geophysical Union.
Vočadlo, L., Alfè, D., Gillan, M. J. & Price, G. D. (2003). *Phys. Earth Planet. Inter.* **140**, 101–105.
Weck, G., Loubeyre, P. & LeToullec, R. (2002). *Phys. Rev. Lett.* **88**, 035504.
Weidner, D. J., Li, L., Davis, M. & Chen, J. (2004). *Geophys. Res. Lett.* **31**, L06621.
Wenk, H.-R., Matthies, S., Hemley, R. J., Mao, H. K. & Shu, J. (2000). *Nature (London)*, **405**, 1044–1047.
Williams, G. P. (1990). *Nucl. Instrum. Methods Phys. Res. A*, **291**, 8–12.
Williams, Q. & Hemley, R. J. (2001). *Ann. Rev. Earth Planet. Sci.* **29**, 365–418.
Xie, X., Minitti, M. E., Chen, M., Mao, H. K., Wang, D., Shu, J. & Fei, Y. (2002). *Geochim. Cosmochim. Acta*, **66**, 2439–2444.
Xu, J. & Mao, H. K. (2000). *Science*, **290**, 783–785.
Xu, J., Mao, H. K., Hemley, R. J. & Hines, E. (2002). *J. Phys. Condens. Matter*, **14**, 11543–11548.
Xu, J. A., Mao, H. K., Hemley, R. J. & Hines, E. (2004). *Rev. Sci. Instrum.* **75**, 1034–1038.
Yan, C., Vohra, Y. K., Hemley, R. J. & Mao, H. K. (2002). *Proc. Nat. Acad. Sci.* **99**, 12523–12525.
Yan, C. S., Mao, H. K., Li, W., Qian, J., Zhao, Y. & Hemley, R. J. (2004). *Phys. Status Solidi A*, **201**, R25–R27.
Yoo, C. S., Cynn, H., Gygi, F., Galli, G., Iota, V., Nicol, M., Carlson, S., Hausermann, D. & Mailhiot, C. (1999). *Phys. Rev. Lett.* **83**, 5527–5530.
Yoo, C. S., Iota, V. & Cynn, H. (2001). *Phys. Rev. Lett.* **86**, 444–447.
Yoo, C. S., Kohlmann, H., Cynn, H., Nicol, M., Iota, V. & LeBihan, T. (2002). *Phys. Rev. B*, **65**, 104103.
Young, D. A. (1991). *Phase Diagrams of the Elements.* University of California Press.
Zha, C. S., Mao, H. K. & Hemley, R. J. (2000). *Proc. Nat. Acad. Sci.* **97**, 13494–13499.
Zha, C. S., Mao, H. K. & Hemley, R. J. (2004). *Phys. Rev. B*, **70**, 174107.
Zou, G., Ma, Y., Mao, H. K., Hemley, R. J. & Gramsch, S. A. (2001). *Rev. Sci. Instrum.* **72**, 1298–1301.